Estimation of contact and disturbance forces and interaction force tracking with an aerial manipulator

Master Thesis

Author(s):
Malczyk, Grzegorz iD

Master Thesis

Estimation of contact and disturbance forces and interaction force tracking with an aerial manipulator

Spring Term 2022

Supervised by:
Maximilian Brunner
Eugenio Cuniato
Dr. Marco Tognon

Author:
Grzegorz Malczyk

ETH

Eidgenössische Technische Hochschule Zürich
Swiss Federal Institute of Technology Zurich

Declaration of originality

The signed declaration of originality is a component of every semester paper, Bachelor's thesis, Master's thesis and any other degree paper undertaken during the course of studies, including the respective electronic versions.

Lecturers may also require a declaration of originality for other written papers compiled for their courses.

_____

I hereby confirm that I am the sole author of the written work here enclosed and that I have compiled it in my own words. Parts excepted are corrections of form and content by the supervisor.

Title of work (in block letters):

> *Estimation of contact and disturbance forces and interaction force tracking with an aerial manipulator*

Authored by (in block letters):
For papers written by groups the names of all authors are required.

Name(s):	**First name(s):**
Malczyk	Grzegorz

With my signature I confirm that
− I have committed none of the forms of plagiarism described in the 'Citation etiquette' information sheet.
− I have documented all methods, data and processes truthfully.
− I have not manipulated any data.
− I have mentioned all persons who were significant facilitators of the work.

I am aware that the work may be screened electronically for plagiarism.

Place, date	**Signature(s)**
28.04.2022, Zürich	*Gregorz Malczyk*

For papers written by groups the names of all authors are required. Their signatures collectively guarantee the entire content of the written paper.

Contents

Preface

This report has been written in the course of the compulsory master project of the Master Programme in Robotics, Systems and Control at ETH Zurich in the spring semester of 2022. During my master thesis, I had the chance to explore and implement possible strategies for contact-based inspection with over-actuated micro aerial vehicles. That was a challenge where I could apply many things I had learned in the past years at ETH Zürich.

I would like to express my thankfulness to the Autonomous Systems Lab at ETH Zürich, especially Prof. Roland Siegwart, for providing an opportunity to work in your group and carry out this project.

Next, I want to thank my supervisors Maximilian Brunner, Eugenio Cuniato and Dr Marco Tognon for allowing me to work on an exciting project. They supported me throughout my thesis, and I could always rely on their competent help when I ran into difficulties. Without them and their tremendous support, the submitted paper would not have been possible.

Lastly, I want to thank my friends and family that always supported me during these months of the project and encouraged me to push myself to achieve my goals during my education.

Abstract

Over-actuated MAVs have received growing attention in recent years as they allow for physical interaction with their environment. Most interaction tasks so far have been conducted in controlled laboratory environments with little to no outside disturbances.

To perform high-accuracy interaction tasks in outdoor conditions, we need a method to reliably distinguish wrenches (i.e. forces and torques) that arise from interaction at the contact point from those that arise from external disturbances (such as aerodynamic effects from wind).

The applicable methods to achieve this depend heavily on the used sensor equipment. Therefore, we propose to use a combination of odometry and force/torque sensors, together with an analytical model of the platform dynamics. Thus we can estimate contact and disturbance wrenches simultaneously.

In this project, we present a model-based filtering method, namely Extended Kalman Filter (EKF). Following this, an estimation framework is designed and implemented in simulation and verified on the physical platform. With a combination of a novel (especially for MAVs) hybrid motion-force controller, we enable physical interaction of such vehicles with the environment under the presence of external disturbance. For a contact-based inspection, we provide the platform with two types of manipulators. Initially, we validate our approach with a simple rigid manipulator and subsequently with a delta arm attached to the vehicle. We prove the ability of the entire control framework in real-world experiments. Thus, we verify the quality of the estimates by comparing them to ground-truth measurements and showcasing possible industrial applications.

Symbols

Symbols

m	mass
J	inertia tensor
$_A p_B$	origin of $\mathcal{F}_B$ expressed in $\mathcal{F}_A$
R_{AB}	orientation $\in \mathrm{SO}(3)$ of $\mathcal{F}_B$ expressed in $\mathcal{F}_A$
$_A v_B$	linear velocity of $\mathcal{F}_B$ expressed in $\mathcal{F}_A$
$_A \omega_B$	angular velocity of $\mathcal{F}_B$ expressed in $\mathcal{F}_A$
b	force/torque sensor bias
$\boldsymbol{F}$	3-axis force vector
$\boldsymbol{\tau}$	3-axis torque vector
$\tilde{\boldsymbol{\tau}}$	wrench vector $[F, \tau] \in \mathbb{R}^{6 \times 1}$
$\hat{\tilde{\boldsymbol{\tau}}}$	estimated wrench vector
$_W \mathbf{g}$	gravity acceleration vector

Indices

x	x axis
y	y axis
z	z axis
W	inertial (world) frame
B	body-fixed (base) frame
S	Rokubi (force/torque sensor) frame
P	workpiece (interaction surface) frame

Acronyms and Abbreviations

ETH	Eidgenössische Technische Hochschule
EKF	Extended Kalman Filter
IMU	Inertial Measurement Unit
OMAV	Over-Actuated Micro Aerial Vehicle

Chapter 1

Introduction

The increasing demand for industrial contact inspection with aerial robots has been rapidly growing over the last few years, coinciding with the development of over-actuated micro aerial vehicles (OMAVs) for aerial interaction. In this project, we strive to extend the existing novel framework. We want to enable an OMAV equipped with a manipulator and force/torque sensor to perform interaction tasks.

1.1 Motivation

Nowadays, most interaction tasks have been conducted in controlled laboratory environments with little to no outside disturbances yet. Therefore, the reliable interaction external wrench estimate becomes crucial. With the latest approach [1], the platform predicted the entire acting external wrench. Subsequently, the vehicle could not distinguish between different external wrench sources (i.e. contact and disturbance wrenches, as highlighted in fig. 1.1). Thus, we aim to provide a reliable estimate of the interaction force at the contact while external disturbances can arise (such as aerodynamic effects from wind). Consequently, the over-actuated MAV can interact and track a provided force reference while also rejecting external disturbances at the same time.

The over-actuated MAVs have received growing attention recently, especially for industrial applications. Thus, a reliable estimate of the existing external wrenches acting on the system can be employed to enhance the higher manipulation capabilities of the flying vehicle. Our next fundamental goal is to ensure high precision and accuracy while executing any manipulation task. The platform, equipped with a rigid manipulator (fig. 1.1), should be able to exert desired force in any direction of the body frame while interacting. Additionally, the proposed framework should also apply to any other manipulator attached to the OMAV to perform various interaction tasks successfully and precisely.

Lastly, we exploit our knowledge about the entire system to explore possible advanced interaction tasks that the platform can achieve. Keeping industrial applications in mind, we aim to execute with our framework not simply contact point operations but also push-and-slide actions under various conditions and configurations.
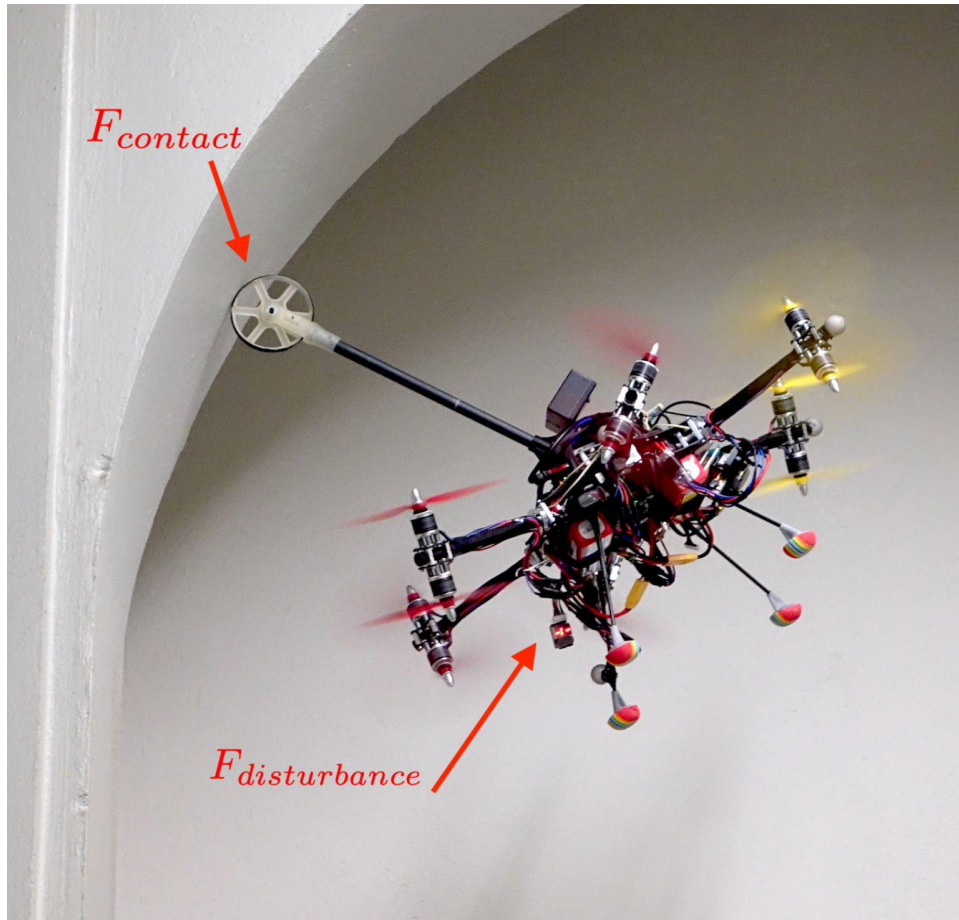
Figure 1.1: External wrenches acting on the flying vehicle

1.2 Related Work

Micro aerial vehicles (MAVs) are small and agile. Furthermore, they are becoming increasingly capable of their compact size. Those platforms are expected to perform a wide variety of tasks, where they are either required to physically interact with the environment for applications such as inspection and manipulation [2], [3] and [4] or fly in close proximity to other flying platforms for applications involving formation flight [5], [6]. In all mentioned situations, the system may experience significant external forces, which are difficult to model but affect the robot's dynamic behaviour. While MAVs have been embraced as a solution for efficient visual inspection of infrastructure [7], contact-based inspection still requires extensive human labour and relies on large supporting inspection equipment. Extending the capabilities of MAVs to perform contact inspection is the next obvious step. Typically these applications demand force-sensing which may be provided with a dedicated force sensor. Thanks to the new developments in sensor technology, several small and lightweight devices have emerged. Thus, a MAV-based inspection becomes a feasible reality [8]. The task remains to tackle combined interaction force control with disturbance rejection on an autonomous MAV.

Researchers have shown numerous applications for robotic systems that use external force and torque estimates as an input to their algorithms and, accordingly,

have developed improved force and torque estimators better suited for the demands of these tasks. A non-linear observer was first applied to estimate external forces and torques by [9] and [10]. These papers highlight many potential applications along with reducing the risk of damage in a collision, tactile mapping, takeoff and landing detection, identifying the material of a surface by colliding with it [9], and impedance control [10], [1] and extended in [11]. Non-linear observers work well in practice if the occurring forces are large and sensor noise is poor. Otherwise, inputs and outputs of the non-linear observer must be carefully filtered since the algorithm is based on a deterministic formulation and does not account for process and sensor noise. Filter tuning can be a complex and time-consuming process. Non-linear state estimation algorithms such as the Extended Kalman Filter (EKF) addressed this issue to handle sensor and process noise.

When aerial vehicles are in interaction with the environment, they need to be able to control at the same time the position at the contact, and the interaction force, preserving the stability of the entire system. A possible control scheme is the hybrid motion/force control method [12] that aims to control the contact force in a direct way. Interaction control techniques with a hybrid control approach have been actively explored since the 1970s for fixed-base manipulators but have not been possible for aerial robots until the past decade. In the flying platform case, the system is controlled by two complementary feedback loops, one for the motion and the other for the interaction force, along the unconstrained and constrained axes respectively. Such a control strategy has been implemented for uni-directional thrust [12] and fully actuated [13] vehicles.

In the state-of-the-art related to aerial physical interaction, one equipped the MAVs platforms with various end-effectors, e.g. rigid links or delta-like manipulators. Those aerial manipulators are specially developed for point contact [14], [15] and sliding tasks [16] or for aerial repair [17].

1.3 Contribution

This thesis presents a unified framework for external wrench estimation and interaction control for flying robots. First, we develop an estimator of the external forces and torques acting on the platform that exploits the control input, state measurements, and the dynamic model of the aerial platform. We propose an Extended Kalman Filter (EKF) tailored to the needs of flying systems, which uses a non-linear model for the hexarotor dynamics. The approach explicitly accounts for sensor noise and imperfections in our flying system and uses singularity-free quaternions to represent the attitude of the hexarotor. Non-linear state estimation algorithms such as the EKF are designed to accurately model sensor and process noise. Many of the tuning parameters are derived directly from the noise properties of the sensors, making them easy to tune. We demonstrate the effectiveness of such an approach in several experiments with an OMAV.

Subsequently, we use this estimate for controlled physical interaction with the environment. For this purpose, we design a Hybrid Motion/Force Controller. The selective impedance control strategy, introduced in [1], is replaced within this project. Two complementary feedback loops control the flying vehicle: the first is responsible for the platform motion, and the other for regulating the contact force with the environment. Thanks to the Hybrid Motion/Force Controller, we ensure accurate position and force tracking while addressing contact constraints carefully.

Together, these algorithms enhance the capabilities of flying robots beyond the current state of the art. We take inspiration from well-established methods from robot manipulator literature and apply them to over-actuated flying robots. Furthermore, we extend the analysis to interaction control under external disturbance influence. But now, one requires a floating base to carry a sensor to precisely exert forces on the environment in any direction while simultaneously rejecting other sources of disturbance. Our approach combines the omnidirectionality of the platform with high wrench exertion capabilities. Thus we eliminate the need for an actuated manipulator arm to enable interaction with the environment. Moreover, we validate the proposed novel interaction framework with a delta manipulator attached to our flying vehicle in addition to the rigid manipulator.

1.4   Outline

This paper is organized as follows. To introduce the reader to the platform, we present the vehicle setup in Chapter 2. In that section, we indicate two possible vehicle configurations, as one equipped the platform with either a rigid manipulator or a delta arm. In Chapter 3.1, an overview of the OMAV control scheme is provided. We elaborate on our approach to external wrench estimation in Chapter 3.2. Subsequently, one develops the Hybrid Motion/Force Controller for physical interaction with the environment in Chapter 3.3. The proposed approach employs the EKF wrench estimate to ensure high accuracy and offset-free contact force tracking. We investigate and show the effectiveness of the presented methods through experiments in Chapter 4, especially demonstrating possible advanced interaction capabilities with our framework. Finally, we conclude and discuss future work in Chapters 5 & 6.

Chapter 2

Problem Definiton

2.1 System Description

This chapter describes the MAV system and hardware. The vehicle used in this work takes the form of a traditional hexarotor with equally spaced arms about the body z-axis. Each propeller group can independently tilted by a dedicated servo motor, allowing various rotor thrust combinations. This tilt action permits high force and torque generation in any direction while maintaining efficient flight in horizontal hover. Double rotor groups provide additional thrust for a compact system. Symmetrically placed rotors balance rotational inertia about the tilt axis to reduce the effort of the tilt motors. The platform structure consists of custom carbon fibre, aluminium, and 3D printed plastic parts. The system is categorized as fully actuated and omnidirectional. The platform uses lithium-polymer batteries for onboard power. Finally, processing occurs on an onboard computer and flight controller.

For interaction control system is equipped with a *Rokubi* 6-axis force/torque sensor[1]. The sensor's small size and mass (230 g) allow integration between the vehicle base and the manipulator, as depicted in fig. 2.1 & fig. 2.3. Initially, the sensor was mounted at the tip of the end-effector. Shifting the device position away from the end-effector enables incorporating additional sensor measurements. With this setup now, we can also sense the torques induced by the contact forces acting at the tip of the manipulator. Additionally, location change reduces the effect of inertial forces and vibration on the sensor measurements. With integrated EtherCAT electronics, no additional processing hardware is required.

2.1.1 Rigid Manipulator

The homogeneous carbon fibre manipulator arm base is rigidly mounted to the *Rokubi* 6-axis force/torque sensor. The *Rokubi* z_S-axis intersects the body origin and is collinear with the x_B-axis. The arm length from the sensor to the end-effector is 0.395 m, and the distance from the body origin to the manipulator's tip is measured to be 0.555 m. The carbon fibre manipulator attached to the force/torque sensor weighs 0.0725 kg. Please refer to Figure 2.1, which presents the entire vehicle setup with marked frames.
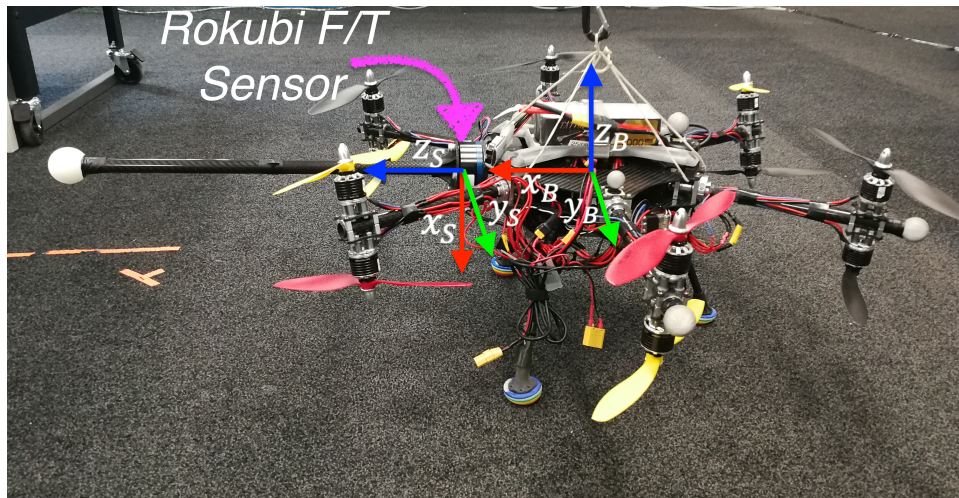
---

[1]https://www.botasys.com/rokubi

Figure 2.1: OMAV with Rigid Manipulator

2.1.2   Delta Manipulator

A parallel 3-DoF delta manipulator base is tightly fixed to the *Rokubi* 6-axis force/torque sensor. The arm is mounted from the bottom of the vehicle, as depicted in Figure 2.2.
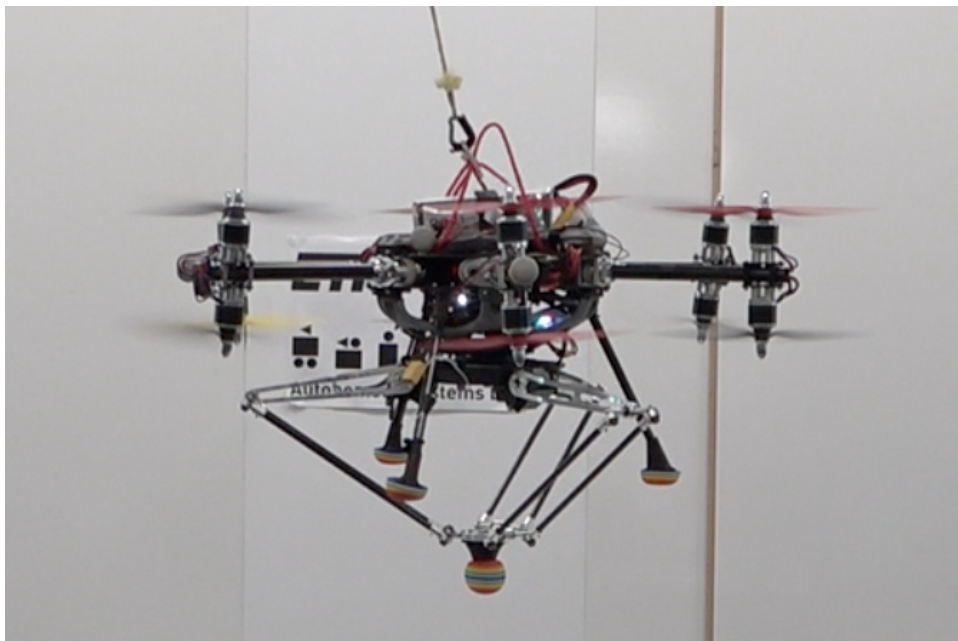

Figure 2.2: OMAV with Delta Arm

In this configuration, the F/T sensor is also located between the OMAV body and the delta arm base to reduce the vibration effects. For reference, we present the entire mounting arrangement of the sensor with the platform in Figure 2.3.

The mounting plate between the flying base and the sensor weighs 30 g The second plate between the F/T sensor and the delta arm motors is 70 g. The two plates
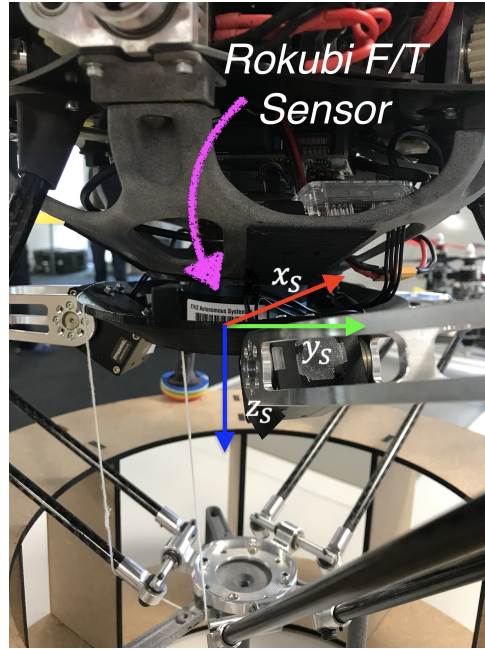
Figure 2.3: Mounting of the F/T Sensor with Delta Manipulator

are thick 0.002 m each. The z_S-axis intersects the body origin and is collinear with
the z_B-axis. Finally, it results in vertical displacement of the delta arm base from
the geometrical OMAV body origin of 32 mm. The complete manipulator assembly
weighs 0.72 kg, of which only 0.28 kg is moving relative to the delta manipulator
mounting base. The delta arm is mounted on a 4.6 kg flying robot, then the pro-
portion of moving to total vehicle mass is less than 5%. Dynamixel M430-W210
motors are selected for their sufficient torque capability and integrated position and
velocity feedback. For a detailed description of the mechanical design and control
framework of delta manipulator, the reader could refer to [18].

2.2   Problem Statement

At this point, before coming to the proposed approach, we summarize and state the
final objectives of the project and the assumptions we made about the interaction
point.

- We extend the existing novel control framework to enable an OMAV equipped
  with a manipulator to perform high-accuracy interaction tasks with the envi-
  ronment.

- For the interaction tasks, a reliable estimate of the interaction force at the
  contact is crucial. But simultaneously, the platform should be capable of
  distinguishing between interaction and external disturbance wrenches, which
  act on the vehicle.

- The main goal is to precisely interact with the environment even in presence
  of external disturbances, such as wind disturbance.

- The interaction point of the platform with the environment is assumed to
  be only at the tip of the manipulator, where only a pure three-dimensional
  contact force acts.

Chapter 3

Approach

The following section demonstrates the approach enabling an OMAV to distinguish between external wrenches acting on the vehicle. Subsequently, we provide a description and implementation of the Hybrid Motion/Force Controller that fuses the external wrench estimate within the control loop. With this type of controller, the flying platform receives the capability to execute various advanced interaction tasks. The specified smooth force/state trajectory proceeds from the motion planner to the controller. Thanks to that, we enable the autonomous accomplishment of the demanded task.

3.1 Controller Structure

First, we briefly discuss the controller structure of the system depicted in Figure 3.1.
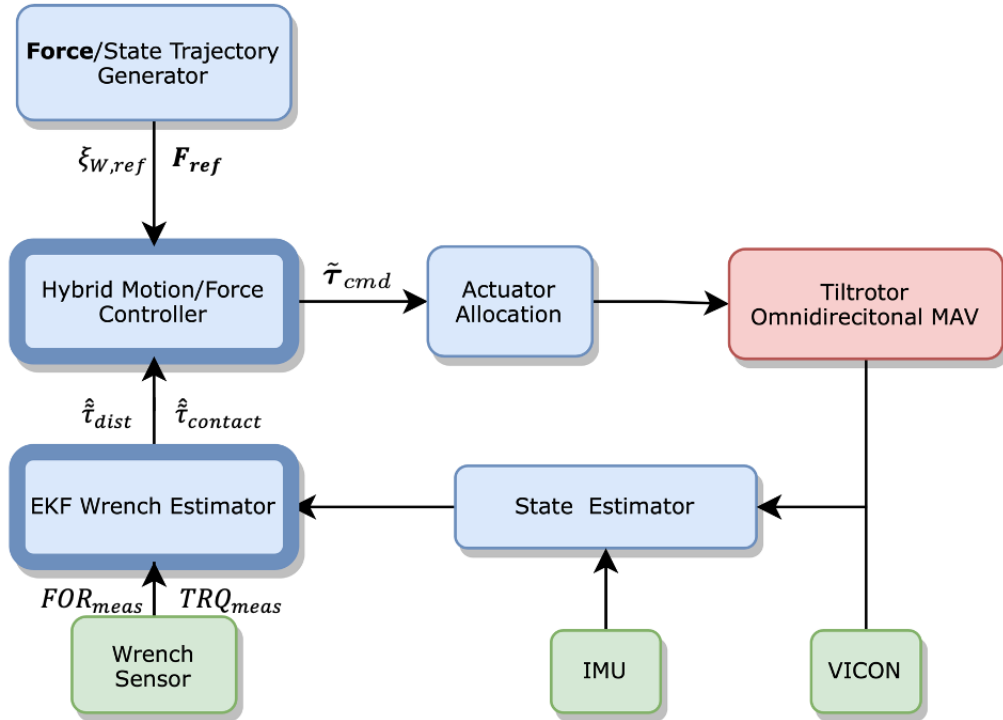
Figure 3.1: Scheme of the proposed controller structure

In fig. 3.1, the red box indicates the physical platform prototype. In green, we mark sensors of the experimental setup and in blue, software segments of the controller framework. Two blue components, highlighted by dark blue contours, indicate the blocks newly introduced within this project.

Based on the IMU measurements and motion capture system *VICON*, the state estimator provides information about the actual state of the system. This data notifies the entire framework about the current platform position, orientation, and twist, i.e. linear and angular velocities of the vehicle.

We extend the former controller structure by introducing additional components. Firstly, we add an EKF Wrench Estimator. This software module enables us to estimate and differentiate between external wrenches acting on the vehicle, which was not possible with the previous controller framework. The wrench sensor, attached to the platform, is placed between the manipulator and the flying base and provides the force and torque (wrench) measurements of the contact force. We assume only one single interaction point with the environment, i.e. the contact point is at the tip of the manipulator. Subject to the F/T sensor wrench measurement, the EKF module estimates disturbance and interaction wrenches accordingly.

Next, we replace the Motion Controller from the former control strategy with a Hybrid Motion/Force Controller. Such an approach enables regulating the vehicle motion and interaction force simultaneously. The controller obtains both EKF wrench estimates and the entire odometry information. Additionally, it receives at each time step a reference trajectory. This trajectory includes requested values for the pose $\boldsymbol{\xi}_{W,ref}$ of the vehicle in the world frame. Besides that, it consists of interaction force reference $\mathbf{F}_{ref}$. Finally, based on all input data to the Hybrid Motion/Force Controller, the final wrench command is computed appropriately to achieve its desired state.

In the upcoming sections, we derive the EKF Wrench Estimator algorithm and formulate the Hybrid Motion/Force Controller law. The resulting system performance of this approach is depicted in Chapter 4.

3.2   EKF Wrench Estimator

The first component of the force and torque estimation algorithm is a simplified model of the hexarotor dynamics. External forces and torques are quantities that cannot be explained by our first-principles hexarotor model but are exerted by external sources such as physical contact or air disturbance. We present a wrench estimation scheme based on the Extended Kalman Filter (EKF) that carefully models the source of process and measurement noise. The two essential steps in the EKF implementation are the prediction and the correction step. The prediction step predicts the state of the OMAV at the next time-step given motor wrench commands and a model of the over-actuated MAV dynamics. In the correction step, we update the current state estimate to explain better the observed vehicle motion. The external force and torque estimates should describe the differences between measurements and the corresponding predicted values, distinguishing between interaction and disturbance wrenches.

3.2.1   Prediction Model

Here, we present the continuous-time model of the omnidirectional hexarotor dynamics, which one exploits to derive the discrete-time model. In our final implementation, we use a discrete-time model to accurately represent the discrete nature of the measurements and inputs and the corresponding uncertainties in the model.

Assumptions

We model the flying vehicle as a rigid body with mass m and $\mathbf{I} \in \mathbb{R}^{3\times3}$ inertia matrix, such that the body axes correspond with the principal axes of inertia. Thrust and drag torques are assumed proportional to squared rotor speeds, which the system achieves instantly without transients. We further expect that tilt motor dynamics are negligible compared to the whole system dynamics, and tilt mechanism backlash and alignment errors are insignificant. Our model neglects aerodynamic effects, which are reasonably small at slow speeds and are estimated by the proposed filter as further disturbances.

Translational Dynamics

Under the assumptions stated above, the continuous-time translational dynamics read:

$$_W\dot{\mathbf{p}} = {}_W\mathbf{v} \, , \tag{3.1}$$

$$_W\dot{\mathbf{v}} = \frac{\mathbf{R}_{W,B}(\mathbf{u}_f + \boldsymbol{\eta}_{u_f} + \mathbf{F}_c) + \mathbf{F}_d}{m} - {}_W\mathbf{g} \, , \tag{3.2}$$

where $_W\mathbf{p} = [x, y, z]^\top$ is the position of the centre of mass of the platform in global world coordinates and $_W\mathbf{v}$ stays for the linear velocity expressed in the global frame. $\mathbf{R}_{W,B}$ represents the rotation matrix from the global frame to the body frame, $\mathbf{F}_c$ the contact force acting on the hexarotor in body coordinates and $\mathbf{F}_d$ the external disturbance force in global coordinates. The vector $_W\mathbf{g}$ describes gravity acceleration in the world frame. The input thrust is $\mathbf{u}_f$ and $\boldsymbol{\eta}_{u_f}$ represents the input thrust process noise.

The process noise in (3.2) is to account for uncertainty in the model of the thrust produced by each propeller. The thrust mapping is derived close to hover and is not accurate when the hexarotor airspeed and attitude are non-zero. Moreover, the measurements of the motor turn rates are quantized which adds quantization

noise to the system. To account for these effects, we add zero-mean Gaussian noise, $\boldsymbol{\eta}_{u_f} \sim \mathcal{N}(0, \mathbf{Q}_{u_f})$ to the nominal thrust with $\mathbf{Q}_{u_f}$ being the corresponding covariance matrix.

The contact forces $\mathbf{F}_c$ are expressed in the body frame and the disturbance forces $\mathbf{F}_d$ in the global frame. We do not assume any specific underlying dynamics for the external forces. We model their dynamics as a random walk, namely:

$$\dot{\mathbf{F}}_c = \boldsymbol{\eta}_c \ , \tag{3.3}$$

$$\dot{\mathbf{F}}_d = \boldsymbol{\eta}_{d,f} \ , \tag{3.4}$$

where both $\boldsymbol{\eta}$'s are zero-mean Gaussian noise vectors, $\boldsymbol{\eta}_c \sim \mathcal{N}(0, \mathbf{Q}_c)$ and $\boldsymbol{\eta}_{d,f} \sim \mathcal{N}(0, \mathbf{Q}_{d,f})$. Each $\mathbf{Q}$'s defines a diagonal covariance matrix respectively. The expected value of each external force does not change over time, but its variance increases. Values farther from the mean become more likely as time passes. This choice for the dynamics of external forces allows the EKF to explain discrepancies between the prediction and measurements by any additional external force acting on the system.

The covariances, $\mathbf{Q}_c$ and $\mathbf{Q}_d$, become the tuning parameters. A smaller covariance indicates that we expect the force to change slowly, and a greater covariance means that we expect it to change quickly. A diagonal noise covariance implies that force components vary independently. Modelling force dynamics as a random walk has proven sufficient to estimate unknown, changing forces.

Rotational Dynamics

The orientation of the body frame with respect to the global frame is represented by the (4×1) unit quaternion $_W\boldsymbol{q} = [q_0, \boldsymbol{q}_v]^\top, \boldsymbol{q}_v \in \mathbb{R}^{3 \times 1}$. To derive the continuous-time equations, we employ an approach presented by Sola et al. [19].

The final rotational dynamics equation reads:

$$_W\dot{\mathbf{q}} = \frac{1}{2}\boldsymbol{\Omega}(_B\boldsymbol{\omega}) \cdot {_W}\mathbf{q} \ , \tag{3.5}$$

$$_B\dot{\boldsymbol{\omega}} = \mathbf{I}^{-1}(\mathbf{u}_t + \boldsymbol{\eta}_{u_t} + \mathbf{r}_{contact} \times \mathbf{F}_c + \boldsymbol{\tau}_d - {_B}\boldsymbol{\omega} \times I_B\boldsymbol{\omega} - \boldsymbol{r}_{CoM} \times {_B}\mathbf{g}m) \ , \tag{3.6}$$

where $_B\boldsymbol{\omega} = [\omega_x, \omega_y, \omega_z]^\top$ is the angular velocity of the platform in the body frame and

$$\boldsymbol{\Omega}(_B\boldsymbol{\omega}) = \begin{bmatrix} 0 & -\omega_x & -\omega_y & -\omega_z \\ \omega_x & 0 & \omega_z & -\omega_y \\ \omega_y & -\omega_z & 0 & \omega_x \\ \omega_z & -\omega_y & -\omega_x & 0 \end{bmatrix} \ . \tag{3.7}$$

Subsequently, the model includes torques induced by interaction forces $\mathbf{F}_c$. The vector $\mathbf{r}_{contact}$ describes the position of the interaction force in the body frame. Since the interaction point is assumed to be at the tip of the manipulator, $\mathbf{r}_{contact}$ represents the end-effector position. Additionally, the model accounts for the torque caused by CoM body offset $\boldsymbol{r}_{CoM}$ with respect to the geometrical centre of the vehicle.

The motors act in pairs to produce a thrust differential that results in a torque, which is conveniently expressed in the body frame, $\mathbf{u}_t = [\tau_x^m, \tau_y^m, \tau_z^m]^\top$. As the command motor torque, $\mathbf{u}_t$, is uncertain for the same reasons as a command thrust, we

model this uncertainty as an additive zero-mean Gaussian noise, $\boldsymbol{\eta}_{u_t} \sim \mathcal{N}(0, \mathbf{Q}_{u_t})$, with (3×3) diagonal covariance matrix, $\mathbf{Q}_{u_t}$.

The external torque, $\boldsymbol{\tau}_{dist}$, which comes from unmodeled external disturbance sources, is expressed in the body frame. Similar to the external disturbance force, $\mathbf{F}_d$, we include the external disturbance torque and model it as a random walk, where $\boldsymbol{\eta}_{d,t}$ is zero-mean Gaussian noise, $\boldsymbol{\eta}_{d,t} \sim \mathcal{N}(0, \mathbf{Q}_{d,t})$, with $\mathbf{Q}_{d,t}$ being the diagonal covariance matrix:

$$\dot{\boldsymbol{\tau}}_d = \boldsymbol{\eta}_{d,t} \ . \tag{3.8}$$

Finally, the state vector of the proposed EKF approach reads:

$$\boldsymbol{x}_{EKF} = [_W\boldsymbol{p}, {_W}\boldsymbol{q}, {_W}\mathbf{v}, {_B}\boldsymbol{\omega}, \mathbf{F}_c, \mathbf{F}_d, \boldsymbol{\tau}_d]^\top \ . \tag{3.9}$$

Thus, the algorithm can differentiate between the interaction force $\mathbf{F}_c$ and the disturbance wrench $\tilde{\boldsymbol{\tau}}_d = [\mathbf{F}_d, \boldsymbol{\tau}_d]$, which may act on the system together.
Following, we discuss the modification of the prediction model according to the type of the manipulator with which we equip the flying based.

Rigid manipulator

The configuration with a rigid manipulator, as depicted in Figure 2.1, provides the following definition of the contact force position vector:

$$\mathbf{r}_{contact} = [r_x, 0, 0]^\top \ , \tag{3.10}$$

where r_x describes the length of the bar and is equal to 0.55[m].

Delta manipulator

For the delta manipulator, the position of the $\mathbf{r}_{contact}$ is the position of the end-effector ball, as depicted in Figure 2.2. Since the 3DoF delta arm's end-effector moves relative to the main flying body, the position vector in the body frame is defined as follows:

$$\mathbf{r}_{contact} = [r_x, r_y, r_z]^\top \ , \tag{3.11}$$

where each vector component is the actual position of the manipulator end-effector expressed in the body frame $\mathcal{F}_B$, and it is obtained based on the current delta arm configuration.

3.2.2 Observation Model

Measurements come from a high-precision, external, camera-based motion capture system *VICON*, which measures the full 6 DoF pose of the vehicle. Additionally, this is fused with the onboard IMU to provide additional odometry measurements. Therefore, we use the measurement of the body position, orientation and twist in the EKF observation model. Finally, we add the *Rokubi* sensor wrench measurement, which consists of three-dimensional force $\mathbf{F}_{c,m}$ and three-dimensional torque $\boldsymbol{\tau}_{c,m}$ measurements. This yields the following definition of the EKF measurement vector:

$$\boldsymbol{z}_{EKF} = [_W\boldsymbol{p}_m, {_W}\boldsymbol{q}_m, {_W}\mathbf{v}_m, {_B}\boldsymbol{\omega}_m, \mathbf{F}_{c,m}, \boldsymbol{\tau}_{c,m}]^\top \ , \tag{3.12}$$

where all the quantities with a subscript m are measurements of the corresponding state components.

We include additive, zero-mean Gaussian noise for the odometry measurements:

$$\begin{aligned}
_W\boldsymbol{p}_m &\to \boldsymbol{w}_{_W\boldsymbol{p}_m} \sim \mathcal{N}(0, \mathbf{G}_{_W\boldsymbol{p}_m}) \,, \\
_W\boldsymbol{q}_m &\to \boldsymbol{w}_{_W\boldsymbol{q}_m} \sim \mathcal{N}(0, \mathbf{G}_{_W\boldsymbol{q}_m}) \,, \\
_W\mathbf{v}_m &\to \boldsymbol{w}_{_W\mathbf{v}_m} \sim \mathcal{N}(0, \mathbf{G}_{_W\mathbf{v}_m}) \,, \\
_B\boldsymbol{\omega}_m &\to \boldsymbol{w}_{_B\boldsymbol{\omega}_m} \sim \mathcal{N}(0, \mathbf{G}_{_B\boldsymbol{\omega}_m}) \,.
\end{aligned}$$

Similar, we define additive, zero-mean Gaussian noise for the contact wrench measurements:

$$\begin{aligned}
\mathbf{F}_{c,m} &\to \boldsymbol{w}_{\mathbf{F}_{c,m}} \sim \mathcal{N}(0, \mathbf{G}_{\mathbf{F}_{c,m}}) \,, \\
\boldsymbol{\tau}_{c,m} &\to \boldsymbol{w}_{\boldsymbol{\tau}_{c,m}} \sim \mathcal{N}(0, \mathbf{G}_{\boldsymbol{\tau}_{c,m}}) \,.
\end{aligned}$$

The diagonal covariance matrices $\mathbf{G}_{\cdot} \in \mathbb{R}^{3\times3}$ depend on the properties of the sensors and devices being used to obtain those measurements. The EKF is easily extendable to incorporate additional measurements such as those from other sensors, e.g. GPS.

The final observation model reads:

$$\boldsymbol{z}_{EKF} = \begin{bmatrix}
\mathbb{I}_{3\times3} & 0 & 0 & 0 & 0 & 0 & 0 \\
0 & \mathbb{I}_{4\times4} & 0 & 0 & 0 & 0 & 0 \\
0 & 0 & \mathbb{I}_{3\times3} & 0 & 0 & 0 & 0 \\
0 & 0 & 0 & \mathbb{I}_{3\times3} & 0 & 0 & 0 \\
0 & 0 & 0 & 0 & \mathbb{I}_{3\times3} & 0 & 0 \\
0 & 0 & 0 & 0 & [\mathbf{r}_{FTS}]_\times & 0 & 0
\end{bmatrix} \boldsymbol{x}_{EKF} + \begin{bmatrix}
\boldsymbol{w}_{_W\boldsymbol{p}_m} \\
\boldsymbol{w}_{_W\boldsymbol{q}_m} \\
\boldsymbol{w}_{_W\boldsymbol{v}_m} \\
\boldsymbol{w}_{_B\boldsymbol{\omega}_m} \\
\boldsymbol{w}_{\mathbf{F}_{c,m}} \\
\boldsymbol{w}_{\boldsymbol{\tau}_{c,m}}
\end{bmatrix} \,, \quad (3.13)$$

where $[\mathbf{r}_{FTS}]_\times$ describes the skew-symmetric matrix of the position of the end-effector with respect to the F/T sensor.

3.2.3 Discrete-Time EKF

For the implementation purposes, we discretize the above-depicted continuous-time dynamics model to get the discrete-time prediction model:

$$\boldsymbol{x}_{EKF}(k) = f(\boldsymbol{x}_{EKF}(k-1), \boldsymbol{\eta}(k-1)) \,.$$

As the measurement model has already its discrete nature, thus, we obtain the following discrete-time EKF equations directly:

$$\begin{aligned}
\boldsymbol{x}_{EKF}(k) &= f(\boldsymbol{x}_{EKF}(k-1), \boldsymbol{\eta}(k-1)) \,, \\
\boldsymbol{z}_{EKF}(k) &= h(\boldsymbol{x}_{EKF}(k), \boldsymbol{w}(k)) \,.
\end{aligned}$$

The initialization procedure sets the state estimate $\hat{\boldsymbol{x}}_m(0)$ and the covariance estimate matrix $\mathbf{P}_m(0)$ under the assumption that no interaction and disturbance wrenches are acting on the platform.

The prediction step of the Extended Kalman Filter is:

$$\hat{\boldsymbol{x}}_p(k) = f(\hat{\boldsymbol{x}}_m(k-1), \mathbf{0}) \ ,$$
$$\mathbf{P}_p(k) = \mathbf{A}(k-1)\mathbf{P}_m(k-1)\mathbf{A}^\top(k-1) + \mathbf{L}(k-1)\mathbf{Q}(k-1)\mathbf{L}^\top(k-1) \ ,$$

where

$$\mathbf{A}(k-1) = \frac{\partial f(\hat{\boldsymbol{x}}_m(k-1), \mathbf{0})}{\partial \boldsymbol{x}} \quad , \quad \mathbf{L}(k-1) = \frac{\partial f(\hat{\boldsymbol{x}}_m(k-1), \mathbf{0})}{\partial \boldsymbol{\eta}} \ ,$$
$$\mathbf{Q}(k-1) = \mathrm{diag}(\mathrm{Var}[\boldsymbol{\eta}(k-1)]) \ .$$

The measurement update step reads:

$$\mathbf{K}(k) = \mathbf{P}_p(k)\mathbf{H}^\top(k)(\mathbf{H}(k)\mathbf{P}_p(k)\mathbf{H}^\top(k) + \mathbf{M}(k)\mathbf{R}(k)\mathbf{M}^\top(k))^{-1} \ ,$$
$$\hat{\boldsymbol{x}}_m(k) = \hat{\boldsymbol{x}}_p(k) + \mathbf{K}(k)(\overline{\boldsymbol{z}}(k) - h_k(\hat{\boldsymbol{x}}_p(k), \mathbf{0})) \ ,$$
$$\mathbf{P}_m(k) = (\mathbb{I} - \mathbf{K}(k)\mathbf{H}(k))\mathbf{P}_p(k) \ ,$$

where

$$\mathbf{H}(k) = \frac{\partial h(\hat{\boldsymbol{x}}_p(k), \mathbf{0})}{\partial \boldsymbol{x}} \quad , \quad \mathbf{M}(k) = \frac{\partial h(\hat{\boldsymbol{x}}_p(k), \mathbf{0})}{\partial \boldsymbol{w}} \ ,$$
$$\mathbf{R}(k) = \mathrm{diag}(\mathrm{Var}[\boldsymbol{w}(k)]) \ ,$$

and $\overline{\boldsymbol{z}}(k)$ represents the recently obtained measurements from the sensors according to Eq.(3.12).

In summary, thanks to the EKF algorithm, the vehicle can reliably distinguish between external wrenches acting on it, as the observability matrix for the presented model with $n = 22$ state variables reads:

$$\mathcal{O}(k) = \begin{bmatrix} \mathbf{H}(k) \\ \mathbf{H}(k)\mathbf{A}(k-1) \\ \mathbf{H}(k)\mathbf{A}^2(k-1) \\ \vdots \\ \mathbf{H}(k)\mathbf{A}^{n-1}(k-1) \end{bmatrix} \quad \Rightarrow \quad \mathrm{rank}(\mathcal{O}(k)) = 22 \ .$$

Therefore, the rank of the observability matrix is equal to the number of the state variables, which implies that all components of the EKF state vector are observable. The contact force estimate $\hat{\boldsymbol{F}}_c$ will be employed in the Hybrid Motion/Force Controller to extend the capabilities of the system by performing high-precision and advanced interaction tasks. Simultaneously, as a result of the EKF approach, the platform obtains further the disturbance wrench estimate $\hat{\tilde{\boldsymbol{\tau}}}_d$. Thus, the OMAV manage to reject current disturbance and the algorithm enhances even the interaction performance.

3.2.4   Force/Torque Sensor

The resulting interaction force is monitored by using a special *Rokubi* force/torque sensor (FTS) located between the manipulator and the flying base. The six-dimensional force and torque (wrench) output of the FTS reads:

$$\tilde{\boldsymbol{\tau}}_{FTS} = [F_x, F_y, F_z, \tau_x, \tau_y, \tau_z]^\top \ .$$

The sensor measurement vector is defined in the body frame $\mathcal{F}_B$.

Due to variations over time, inherent in most electronic components, and considering changes in the operating temperature, drift currents can occur, which results in biased readings. The bias in each force/torque component may be positive or negative. We assume that it does not change significantly between consecutive EKF initializations.

Furthermore, the manipulator mass produces a force $\mathbf{F}_g$ due to its gravity, which contributes to the FTS measurement, and varies, depending on the flying platform orientation in the global reference frame.

Thus, the force/torque output of the FTS does not give us directly the contact force $\mathbf{F}_c$. Instead, the FTS wrench measurement is defined by the following Equation:

$$\tilde{\boldsymbol{\tau}}_{FTS} = \tilde{\boldsymbol{\tau}}_b + \tilde{\boldsymbol{\tau}}_g + \tilde{\boldsymbol{\tau}}_c + \tilde{\boldsymbol{\tau}}_w \; , \tag{3.14}$$

where $\tilde{\boldsymbol{\tau}}_b$ represents the FTS wrench bias, $\tilde{\boldsymbol{\tau}}_g$ is the manipulator gravity wrench, $\tilde{\boldsymbol{\tau}}_c$ is the interaction wrench. The vector $\tilde{\boldsymbol{\tau}}_w$ describes the FTS output noise and the FTS output due to vibration and inertial forces. This part of the FTS wrench measurement is tackled as a measurement sensor noise within the observation model (Sec. 3.2.2) of the EKF algorithm as follows:

$$\tilde{\boldsymbol{\tau}}_w = \left[\boldsymbol{w}_{\mathbf{F}_{c,m}}, \boldsymbol{w}_{\boldsymbol{\tau}_{c,m}} \right]^\top \; , \tag{3.15}$$

where the $\boldsymbol{w}_\cdot$ are the corresponding measurement noise vectors.

According to Equation (3.13), the interaction wrench in the body frame used in the EKF algorithm reads:

$$\tilde{\boldsymbol{\tau}}_c = \begin{bmatrix} \mathbf{F}_{c,m} \\ \boldsymbol{\tau}_{c,m} \end{bmatrix} = \begin{bmatrix} \mathbf{F}_{c,m} \\ \mathbf{r}_{FTS} \times \mathbf{F}_{c,m} \end{bmatrix} \; ,$$

where $\mathbf{r}_{FTS}$ describes the end-effector position with respect to the sensor. Furthermore, we assume that at the contact point no pure torques appear.

The goal is to compute the constant bias wrench $\tilde{\boldsymbol{\tau}}_b$, and the varying gravity wrench $\tilde{\boldsymbol{\tau}}_g$, for arbitrary FTS orientations and corresponding platform configurations. Thanks to that, we can exploit the contact wrench measurements $\tilde{\boldsymbol{\tau}}_c$ in the EKF wrench estimator while modelling FTS noise directly in the EKF, as stated in Equation (3.15).

Gravity compensation

Since the manipulator mass m_m is known, then the estimated force and torque due to gravity, for an arbitrary robot configuration, is equal to

$$\hat{\tilde{\boldsymbol{\tau}}}_g = \begin{bmatrix} m_m \mathbf{R}_{W,B}^\top {}_W \mathbf{g} \\ m_m \mathbf{r}_{CoM_{FTS}} \times (\mathbf{R}_{W,B}^\top \; {}_W \mathbf{g}) \end{bmatrix} \; ,$$

where ${}_W\mathbf{g}$ is the known gravity constant vector, and the rotation matrix $\mathbf{R}_{W,B}^\top$ defines the FTS frame orientation in the global world frame and is known. The position vector $\mathbf{r}_{CoM_{FTS}}$ describes the position of the actual manipulator CoM in the body frame. For the OMAV with the rigid manipulator, this position vector remains constant. However, while the vehicle is equipped with the delta arm, we need to estimate the current CoM position. Thus, the system computes this quantity on-flight

based on the actual manipulator arm configuration. Finally, the gravity compensation vector $\hat{\tilde{\boldsymbol{\tau}}}_g$ is employed to correct the raw FTS wrench measurement (Eq. 3.14).

Additionally, thanks to obtaining the actual CoM position of the manipulator, we can account for the modelling errors and continuously correct the vehicle's centre of mass. It enhances the estimate accuracy as we introduced the vehicle CoM offset in the prediction model of the EKF algorithm. Thus, we do not experience any change in the estimate of the disturbance and interaction wrench while the end-effector moves relative to the flying base, namely when the delta arm is attached to the system.

Bias estimation

The constant sensor bias is computed while initiating the EKF algorithm. Under the assumption that it does not change over time, we obtain $\hat{\tilde{\boldsymbol{\tau}}}_b$ as the average of the measurements over the predefined cycle to get bias-free measurement readings. Furthermore, we assume that during this procedure, the vehicle does not interact with the environment, i.e. $\tilde{\boldsymbol{\tau}}_c = \mathbf{0}$, and only the manipulator gravity wrench influences the sensor measurement.

3.3   Hybrid Motion/Force Controller

In this section, we present the controller to employ the external wrench EKF estimates. Thus we enable the OMAV to interact with the environment and reject any current disturbance if they occur. We extend the interaction capabilities of the controller for the over-actuated micro aerial vehicle presented in [11].

3.3.1   Force/State Trajectory Generation

We wish to outline the high-level control structure at the beginning of this chapter. Each interaction task is described as a collection of specific constrained subsequent set-points. Each set-point consists of information about desired vehicle position and attitude. Additionally, it holds the transformation matrix of workpiece surface $_W\mathbf{T}_P$ and the reference normal force $\mathbf{F}_{ref}$ to the surface in the workpiece frame $\mathcal{F}_P$. The transformation matrix $_W\mathbf{T}_P$ defines the actual position and orientation of the workpiece frame in the global world frame. We use polynomial trajectory interpolation [20] and nonlinear optimization as described in [21] to obtain smooth paths for the platform. Then the polynomial trajectory is sampled at 100 Hz and passed to the controller as an array of timestamped set-points. Compared to [11], we do not require that the OMAV needs to stay aligned with workpiece surface normal, which is tackled in Section 3.3.5. Finally, the Hybrid Motion/Force Controller receives the smooth vehicle trajectory as a reference to track.

3.3.2   Operational Space Control

There exist many situations where the robot should apply a force in some directions while it needs to move in other directions. An example is polishing a surface, whereby the robot applies a specific pressure force in the normal direction and controls the motion in all other directions. To achieve this capability on the flying vehicles, we make use of so-called operational space control. Following the work of Khatib et al. [22], we can define selection matrices $\mathbf{S}_M$ and $\mathbf{S}_F$ for the motion and force directions, yielding the combined control problem:

$$\tilde{\boldsymbol{\tau}}_{cmd} = \mathbf{S}_M\tilde{\boldsymbol{\tau}}_m + \mathbf{S}_F\tilde{\boldsymbol{\tau}}_f \;, \tag{3.16}$$

where $\tilde{\boldsymbol{\tau}}_m$ is the motion control input computed according to Bodie et al. [23]. The wrench vector $\tilde{\boldsymbol{\tau}}_f$ is the interaction force control input, which will be discussed in Section 3.3.4.

Following [22], we define specification matrices for position and orientation:

$$\boldsymbol{\Sigma}_p = \begin{bmatrix} \sigma_{px} & 0 & 0 \\ 0 & \sigma_{py} & 0 \\ 0 & 0 & \sigma_{pz} \end{bmatrix} \quad , \quad \boldsymbol{\Sigma}_r = \begin{bmatrix} \sigma_{rx} & 0 & 0 \\ 0 & \sigma_{ry} & 0 \\ 0 & 0 & \sigma_{rz} \end{bmatrix}, \tag{3.17}$$

where σ_i are binary numbers assigned the value 1 when a free motion is specified along (linear) or around (rotation) specific axis, and zero otherwise.

In case the contact force coordinate frame is rotated with respect to the inertial body frame described by the rotation transformation matrix $\mathbf{R}$, we need to transform the selection matrix. The two selection matrices $\mathbf{S}_F$ and $\mathbf{S}_M$ are then defined

as:

$$\mathbf{S}_M = \begin{bmatrix} \mathbf{R}^\top \boldsymbol{\Sigma}_p \mathbf{R} & \mathbf{0} \\ \mathbf{0} & \mathbf{R}^\top \boldsymbol{\Sigma}_r \mathbf{R} \end{bmatrix} \quad , \quad \mathbf{S}_F = \begin{bmatrix} \mathbf{R}^\top (\mathbb{I}_3 - \boldsymbol{\Sigma}_p) \mathbf{R} & \mathbf{0} \\ \mathbf{0} & \mathbf{R}^\top (\mathbb{I}_3 - \boldsymbol{\Sigma}_r) \mathbf{R} \end{bmatrix}.$$

(3.18)

In our approach, the rotation transformation matrix $\mathbf{R}$ is extracted from the transformation matrix $_W \mathbf{T}_P$ that the planner provides with a generated trajectory. Thus, it holds:

$$\mathbf{R} = \mathbf{R}_{P,B}$$

3.3.3 Motion Control

For the motion control, we use the PD position and attitude controller. This control approach enables achieving both force- and pose-omnidirectionality with highly dynamic capabilities, while maintaining high efficiency in hover by nature of its six actuated tilt arms. The controller generates an appropriate motion control action $\tilde{\boldsymbol{\tau}}_m$ which is fused to the Hybrid Controller, as described in (3.16). The detailed description of the 6 DOF geometric control that is robust to singularities can be found in [23].

3.3.4 Interaction Force Control

We introduce and design a force controller in the body coordinate frame within this project. This approach enables the computation of the necessary force control wrench command $\tilde{\boldsymbol{\tau}}_f$ to the system. Then it is fused according to Equation (3.16). As a result, the vehicle can perform advanced interaction tasks defined by the predefined interaction task trajectories. The interaction force control implies translating a six-dimensional vehicle control wrench command $\tilde{\boldsymbol{\tau}}_f$ to the three-dimensional contact force output $_B\mathbf{F}_c$ at the tip of the manipulator, as depicted in Figure 3.2.
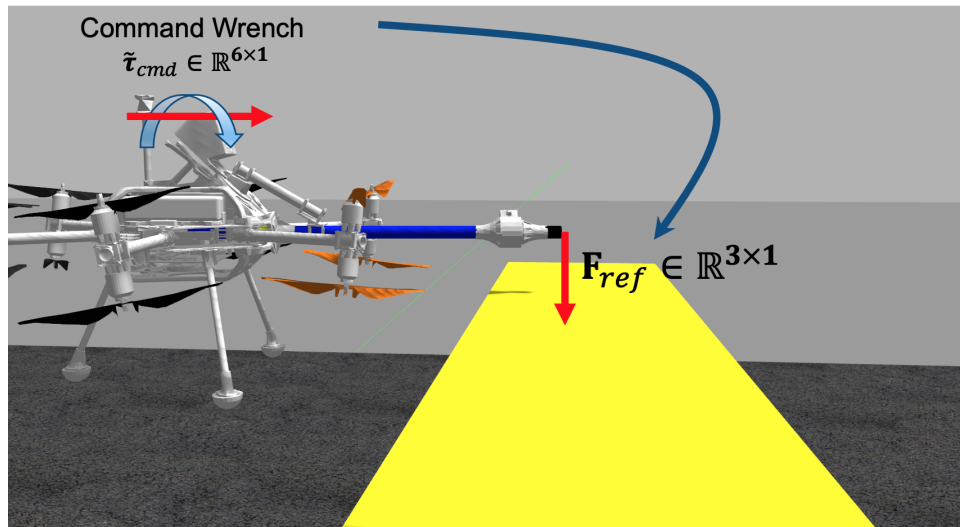

Figure 3.2: Relation between robot wrench command and end-effector interaction force.

This mapping is described by the Jacobi matrix and reads as follows:

$$\tilde{\boldsymbol{\tau}}_f = \mathbf{J}^\top {}_B\mathbf{F}_{ref} = \begin{bmatrix} \mathbb{I}_{3\times 3} \\ [\mathbf{r}_{contact}]_\times \end{bmatrix} {}_B\mathbf{F}_{ref} \tag{3.19}$$

where $[\mathbf{r}_{contact}]_\times$ is the skew-symmetric matrix of a contact force position vector $\mathbf{r}_{contact}$ defined in Eq. (3.10) & (3.11) for each manipulator individually.

Thanks to the previously mentioned mapping, we establish an interaction force control law to regulate the contact force in the body frame. The law consists of feedforward with feedback control action terms to track the desired reference contact force ${}_B\mathbf{F}_{ref}$. The final control action reads:

$$\tilde{\boldsymbol{\tau}}_f = \mathbf{J}^\top ({}_B\mathbf{F}_{ref} + k_p\mathbf{e}_c + k_i \int \mathbf{e}_c \mathrm{dt}) \tag{3.20}$$

where k_p and k_i are positive, constant gains of the PI controller on the error of the contact force $\mathbf{e}_c$. The controller computes the force error accordingly:

$$\mathbf{e}_c = {}_B\mathbf{F}_{ref} - {}_B\hat{\mathbf{F}}_c \tag{3.21}$$

with ${}_B\hat{\mathbf{F}}_c$ is an estimate of the interaction force in the body frame provided by the EKF algorithm.

3.3.5   Offset-Free Reference Tracking

As stated in Section 3.3.1, one defines the initial reference of the contact force $\mathbf{F}_{ref}$ in the workpiece frame. Therefore to exploit the above-described force controller, we need to express the force reference in the body frame instead. Thus, we get:

$$_B\mathbf{F}_{ref} = \mathbf{R}_{P,B}^\top \ \mathbf{F}_{ref} \tag{3.22}$$

where $\mathbf{R}_{P,B}$ represents the rotation from the workpiece frame to the body frame.

Following the example of a robot polishing a surface, the vehicle can only employ one direction (either linear or angular) to control the normal force while still controlling the motion in all other directions. Thus, the platform does not lose its authority position. We define the selection matrices in the workpiece frame, but the control of the interaction force occurs in the body frame. Therefore we need to recompute the force reference signal ${}_B\mathbf{F}_{ref}$, to account for misalignment between them, as we strive to perform offset-free reference force tracking even if the platform is not fully aligned with its workpiece surface. Thanks to the omnidirectionality of our flying platform, and simultaneously depending on the robot's pose with respect to the interaction surface, we enable either the position change or an attitude change to exert specific contact reference. Therefore, the flying vehicle can pitch, roll or yaw to track forces that are not along the leading axis of the manipulator. We presented an example of such a situation in Figure 3.2, where the robot can exert the interaction force by adjusting its pitch angle appropriately.

Based on the ${}_B\mathbf{F}_{ref}$, we select a direction ζ in the body frame, which contributes the most to the normal force. In order to perform offset-free tracking of the reference force, we take the EKF contact force estimate in uncontrolled directions and compute its influence on the normal force to the surface. This yields the following

new reference in the perpendicular direction $\mathbf{F}_{ref}^{new}$, defined in the workpiece frame:

$$\mathbf{F}_{ref}^{new} = \mathbf{F}_{ref} - \mathbf{R}_{P,B} \ \hat{\mathbf{F}}_c^{\zeta} \tag{3.23}$$

where $\mathbf{R}_{P,B}$ is the rotation matrix from the workpiece to the body inertial frame.

Furthermore, considering the above new normal force reference, we find the appropriate reference value in the controlled direction $_B\mathbf{F}_{ref}^{new}$, such that the reference force $\mathbf{F}_{ref}$ is tracked offset-free. The approach employs projecting a reference force $_B\mathbf{F}_{ref}^{new}$ in the controlled direction ζ on the newly found reference vector $\mathbf{F}_{ref}^{new}$. It is achieved by solving the following equation:

$$||\mathbf{F}_{ref}^{new}|| = ||_B\mathbf{F}_{ref}^{new}||\cos(\theta) \tag{3.24}$$

where θ is the angle between the axis of the controlled force ζ and the normal direction to the interaction surface.

After obtaining the new reference force in the body frame, $_B\mathbf{F}_{ref}^{new}$, this value is forwarded to the Interaction Force Controller to track the contact force without any offset.

Considering the actual ζ and the current manipulator configuration, we define the selection matrix entries from Eq. (3.17). For reference, we state below the binary values of the entries which are non-zero for each configuration:

Rigid manipulator

$$\zeta = x_B\text{-axis} \quad \rightarrow \quad \text{Force Control along } x_B\text{-axis} \quad \rightarrow \quad \sigma_{px} = 1$$
$$\zeta = y_B\text{-axis} \quad \rightarrow \quad \text{Force Control around } z_B\text{-axis} \quad \rightarrow \quad \sigma_{rz} = 1$$
$$\zeta = z_B\text{-axis} \quad \rightarrow \quad \text{Force Control around } y_B\text{-axis} \quad \rightarrow \quad \sigma_{ry} = 1$$

Delta manipulator

$$\zeta = x_B\text{-axis} \quad \rightarrow \quad \text{Force Control around } y_B\text{-axis} \quad \rightarrow \quad \sigma_{ry} = 1$$
$$\zeta = y_B\text{-axis} \quad \rightarrow \quad \text{Force Control around } x_B\text{-axis} \quad \rightarrow \quad \sigma_{rx} = 1$$
$$\zeta = z_B\text{-axis} \quad \rightarrow \quad \text{Force Control along } z_B\text{-axis} \quad \rightarrow \quad \sigma_{pz} = 1$$

3.3.6 Transition Between Several Workpieces

An additional feature to address is how to handle the transition between subsequent interaction surfaces. As the trajectory plan contains the transformation of the workpiece frame, we propose the following approach. For the transition phase, we specify two consecutive set-points. They describe identical vehicle position, attitude, and desired normal force to the surface but differ only in the interaction surface frames. The planner generates a smooth trajectory between this pair of set-points (see Section 3.3.1). In that case, the planner provides a smooth rotation from one interaction workpiece frame to the next frame while not changing the vehicle pose or reference normal force. Thus, with correctly defined set-points, the platform can easily transition between subsequent workpieces to complete even more advanced interaction tasks, e.g. polishing a rectangular profile.

3.3.7   Disturbance rejection

At the end of this chapter, as we showcase how the EKF contact force estimate has been used within the Hybrid Motion/Force Controller and following Figure 3.1, we wish to demonstrate how the platform incorporates the information about the current disturbance wrench. We feed the EKF disturbance estimate, $\hat{\tilde{\boldsymbol{\tau}}}_d$, to the hybrid controller and update the wrench command $\tilde{\boldsymbol{\tau}}_{cmd}$ from Eq. (3.16). Then it is sent to the Actuator Allocation Module. The final wrench command reads:

$$\tilde{\boldsymbol{\tau}}_{cmd} = \tilde{\boldsymbol{\tau}}_{cmd} - \hat{\tilde{\boldsymbol{\tau}}}_d$$

Thus, the platform is able to counter-react on the occurring disturbances immediately after it receives current disturbance estimate.

Chapter 4

Experiments

4.1 Experimental Setup

Through a series of experiments, we demonstrate the new capabilities and applications of the system. State estimation for the experiments in this paper is carried out by fusing onboard inertial measurement unit (IMU) data with external motion capture information from a VICON system in an indoor arena. The manipulator (either rigid manipulator or delta arm) is tightly mounted to the omnidirectional flying robot. Reflective marker constellations are installed on the flying base for state estimation, on the manipulator for ground truth position data and for the initial calibration of the manipulator. A safety tether is connected loosely to the robot and minimally affects results. The Hybrid Controller and EKF estimator are implemented in C++ in the Robot Operating System (ROS) framework. A video showcasing the experiments is available as supplementary material.

The experiments in this section are designed to demonstrate the following:

- System response to an external disturbance in a free flight.

- Force control in interaction.

- Push-and-slide tracking on a planar surface while rejecting disturbances and controlling interaction force.

- Ability to interact with complex surfaces

We tune the EKF Wrench Estimator parameters to get an accurate and fast estimate such that it can be employed in the Hybrid Motion/Force Controller to perform advanced interaction tasks. During all experiments, despite the manipulator type used, the PI interaction force controller operates with the hand-tuned gains, which provide stable contact initiation and accurate tracking performance.

4.2   Disturbance in a Free Flight

Firstly, we show the system response to an external disturbance when in free flight. In order to simulate an undesired and invisible disturbance (such as a wind gust), to which the system should react with strong disturbance rejection, we perturb the system with a virtual force. Additionally, to simulate an external disturbance, we also tie a cord to the flying base from the top of the vehicle, which is aligned with the z-axis of the body frame $\mathcal{F}_B$. The other end of the tether is pulled manually to generate an external disturbance wrench. We command the system to hold a reference pose in free flight.

Virtual Disturbance

In the first test, we perturb the vehicle with a virtual three-dimensional force to demonstrate the ability of the framework to accurately estimate the occurring disturbances while also being able to appropriately and quickly reject them. In fig. 4.1, on the right, we plot an applied virtual force as disturbance and corresponding EKF estimate, while on the right side, the vehicle's position. All quantities are expressed in the world frame, and the three-dimensional time-varying disturbance force is applied in a period between 25 and 70 seconds. Firstly, we perturb the system virtually along the x-direction, following the y-direction and z-direction as shown in Figure 4.1.
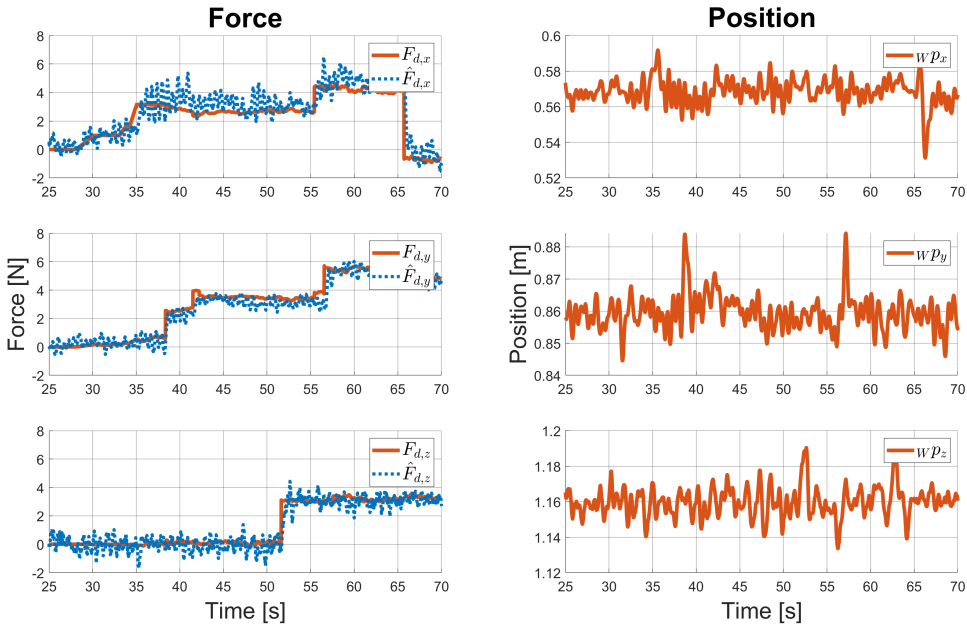
Figure 4.1: Virtual Disturbance in a Free Flight

The framework accurately estimates the current virtual force disturbance applied to the system, which is in the range of 0 up to 6 N. Simultaneously, the disturbance rejection is employed such that the vehicle should hold its initial reference pose even in presence of the virtual disturbance. As presented in Figure 4.1, the vehicle position varies less than 0.03 m when the time-varying three-dimensional force disturbance acts on the system.

Rope Pull Disturbance

In this test scenario, with results shown in fig. 4.2, two pulls on the rope are made for each test. In test 1, we pull vertically on a tether. Thus, especially the disturbance force estimate in the z-direction changes. Subsequently, the next test, namely 2, was performed while the disturbance rejection had been activated, marked with a grey vertical line in the plot. The disturbance rejection is conducted based on the EKF disturbance wrench estimate, as described in Section 3.3.7.
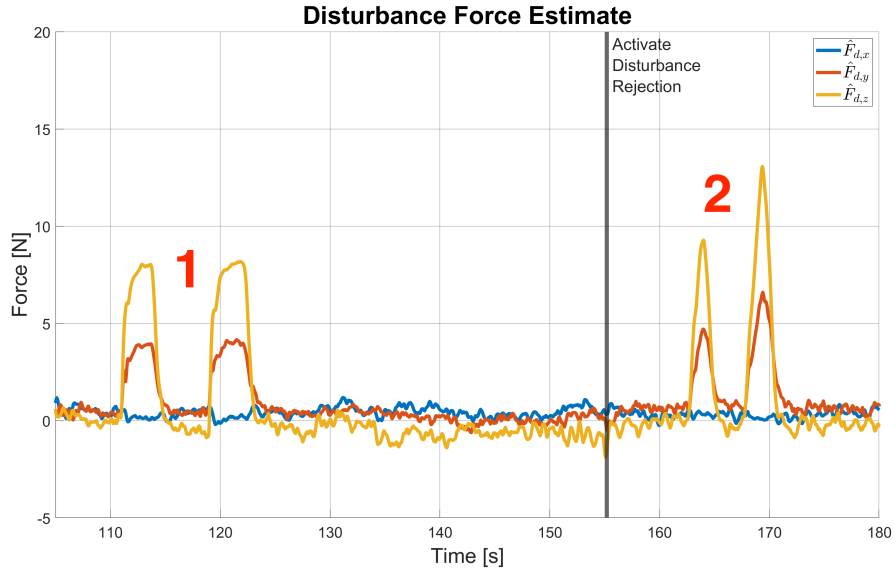
Figure 4.2: Rope Pull Disturbance - EKF Force Estimate

Results from Figure 4.3 show the vertical movement of 0.2 m under a lateral disturbance force of around 10 N, while the disturbance rejection was inactive. After enabling it, the vertical movement has been reduced to less than 0.05 m, demonstrating an ability to actively reject large force disturbances.
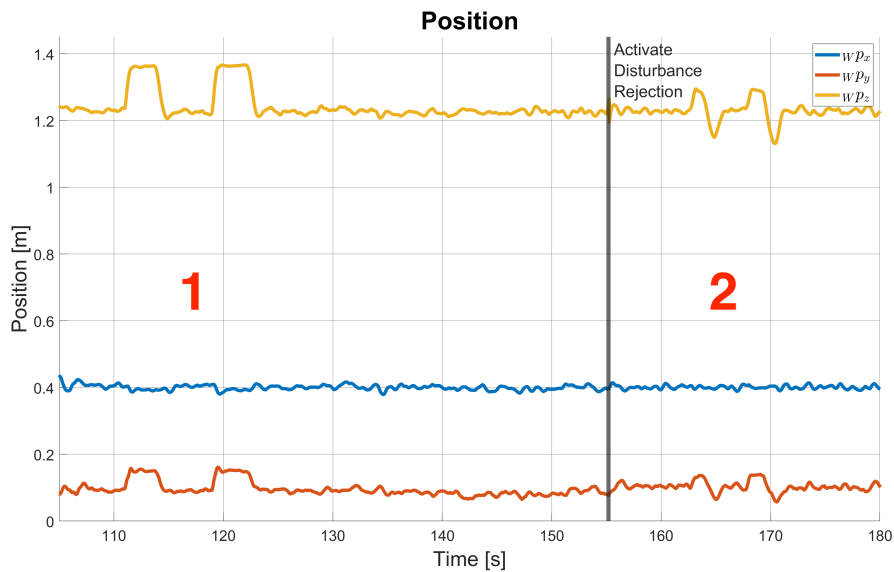
Figure 4.3: Rope Pull Disturbance - Position

4.3 Gravity Compensation

Before coming to the interaction tasks, we examine how the gravity compensation for a reliable wrench estimate is crucial. Principally, when we use the vehicle setup with a delta arm. With this configuration, as the end-effector moves relative to the flying base, the CoM of the delta manipulator and, likewise, of the entire vehicle, change. Thus, this manipulator motion affects the F/T sensor readings. As the manipulator mass does not change, the end-effector movement influences only the torque measurement of the sensor, as presented in the plot below, while the platform was hovering and did not interact with the environment. We commanded the end-effector thrice to execute a triangular path relative to the flying base.
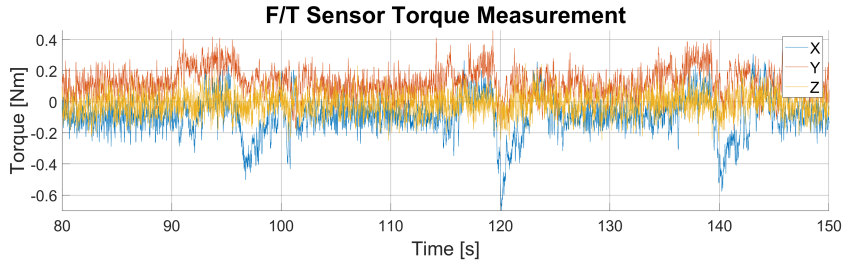
Figure 4.4: Raw F/T Sensor measurement in the body frame

As shown in Figure 4.4, we have to account for the manipulator gravity wrench in the F/T sensor measurement and compensate for a relative end-effector position change. Thus, the EKF estimates are not affected by the end-effector movement, and the gravity compensation becomes essential while performing high-accuracy interaction tasks. In a free flight, the contact force and disturbance torque EKF estimate should remain close to 0 as the system does not interact with the environment.
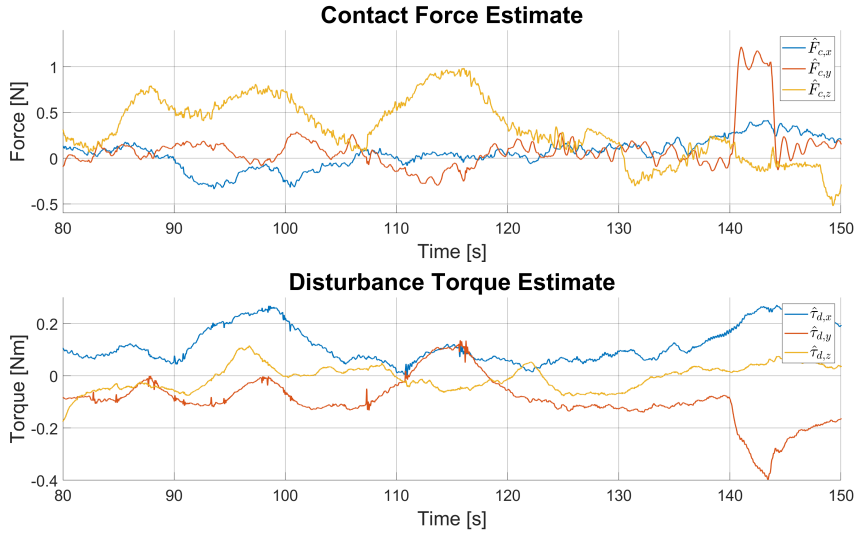
Figure 4.5: EKF Wrench Estimate without Gravity Compensation

Thanks to the approach presented for the gravity compensation, we obtain exactly the EKF estimates, which do not significantly change while the end-effector moves relative to the flying base, especially while the vehicle is in a free flight. The resulting estimated external wrench values are depicted in Figure 4.6.
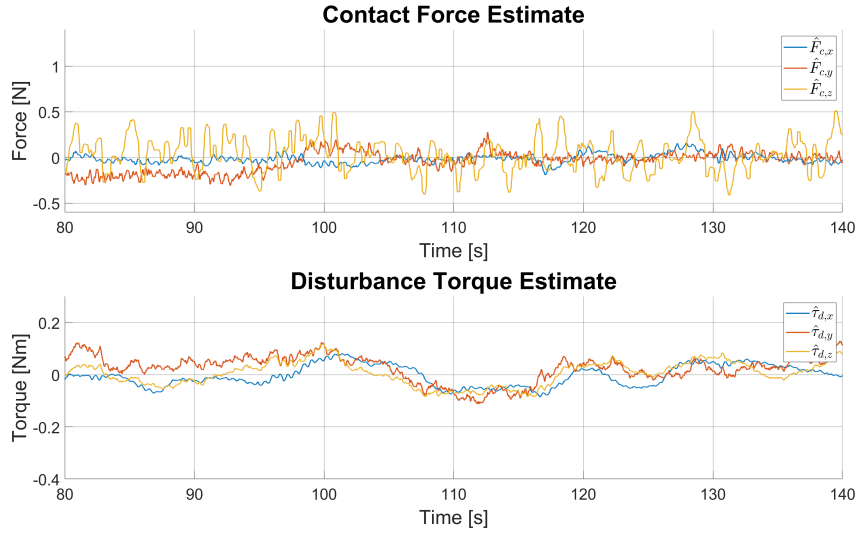
Figure 4.6: EKF Wrench Estimate with Gravity Compensation

Thus, the gravity compensation allows us to provide the EKF with a correct contact wrench measurement and enables us to perform high-accuracy interaction tasks which will be demonstrated in the next section.

Additionally, we depict an offset position of the vehicle's centre of mass (CoM) for reference in Figure 4.7. In the presented experiment, the end-effector moves relative to the flying base mostly along the x and y axes. Simultaneously, the system recomputes the final platform CoM offset as a weighted sum of the manipulator CoM and the pure OMAV CoM. In the plot, we mark in blue the new vehicle CoM and in orange, the platform CoM computed while the manipulator is in its rest configuration. Although, as observed in Figure 4.7, the change in the centre of mass does not vary much (order of [mm]), it has a significant influence on the wrench sensor measurement (Figure 4.4), yielding a non-zero EKF estimate of the contact force and disturbance torque in a free flight (Figure 4.5).
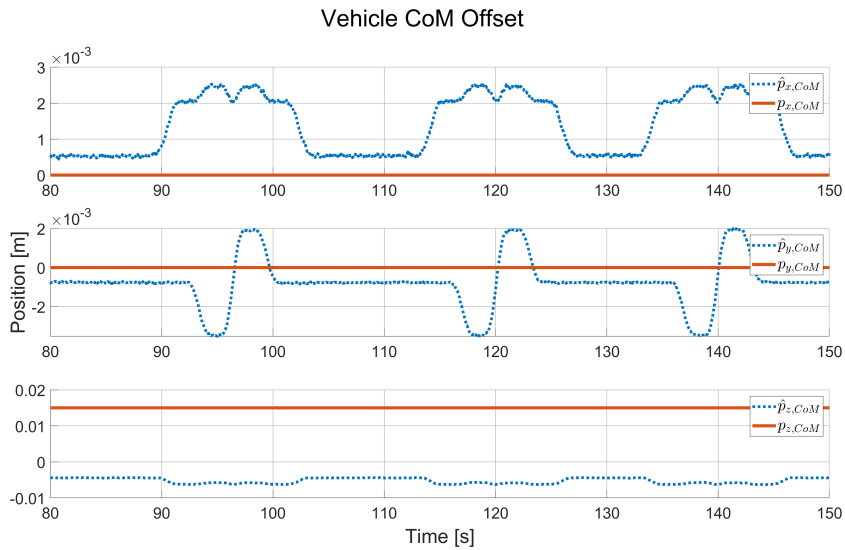
Figure 4.7: Position of the vehicle CoM

4.4 Hybrid Motion/Force Control

In this chapter, we demonstrate the capabilities of the Hybrid Motion/Force Controller for precision interaction with the environment even while external disturbances occur. The controller is validated in a set of experiments in an indoor controlled laboratory environment. In tests, we employ both platform configurations, namely with a simple rigid manipulator and delta parallel arm.

4.4.1 Exponential Moving Average Filter

For estimation purposes, we are interested in the final EKF parameters, which accurately estimate the external wrenches acting on the flying platform. However, the EKF contact force estimate is employed to recompute the offset-free normal force reference as discussed in Section 3.3.5.

Thus, the reference signal acquires the noisy nature resulting from the final EKF parameters tuning. Afterwards, this signal is fed to the Interaction Force Controller (Sec. 3.3.4). In order to provide the PI force controller with a smooth reference, we apply an exponential moving average filter on the offset-free controller input signal. Such an approach enhances the transition phase between free flight and interaction and yields stable contact initiation.

4.4.2 Interaction with Delta Arm

First, we equipped an over-actuated flying vehicle with a delta manipulator attached at the bottom of the flying base. For reference, we present the platform in its rest position in Figure 4.8.

Figure 4.8: OMAV with a Delta Arm in Rest Position

Sliding Along Surface

In this experiment, we evaluate the ability of the system to maintain the normal orientation to a table, rejecting disturbances from virtual forces when tracking a desired normal interaction force. Additionally, we test the ability to distinguish between external wrenches acting on the platform. The table is positioned in a known location, and a trajectory traces an L-shape path for the vehicle along the table while the end-effector position is fixed with respect to the flying base. The desired motion plan contains the normal force reference to the interaction surface as well as the position and orientation of the table in the world global frame. The end-effector is equipped with a rubber ball with no additional compliance element. We depict the experimental setup with a marked L-shaped trajectory in Figure 4.9.
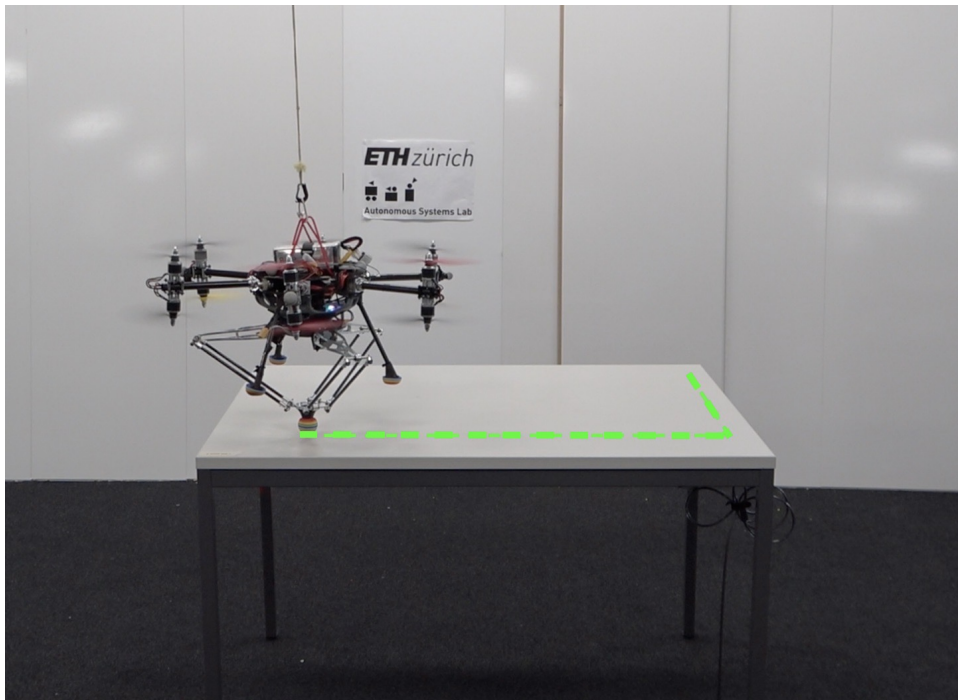
Figure 4.9: L-Shaped Trajectory with Fix End-Effector

Normal force tracking results for this experiment are presented in Figure 4.10, marked in blue the interaction contact force EKF estimate and the reference normal force in orange. The platform performs described L-shaped trajectory twice. In the first attempt, the platform interacts with a table without any external disturbance occurring, while in the second run we apply three-dimensional virtual force disturbance. The time when we employ the virtual perturbation is marked with a yellow background. Thus, we show the framework's ability to distinguish between external wrenches acting on the system.

Without introducing any change in the controller, the system can handle transitions in and out of contact with good stability and without significant difference in tracking on the surface plane. The single noticeable loss of the force tracking is marked with a pink ellipsoid. In this period, we apply a 5N virtual force disturbance along the perpendicular direction to the surface, i.e. along the z-axis.
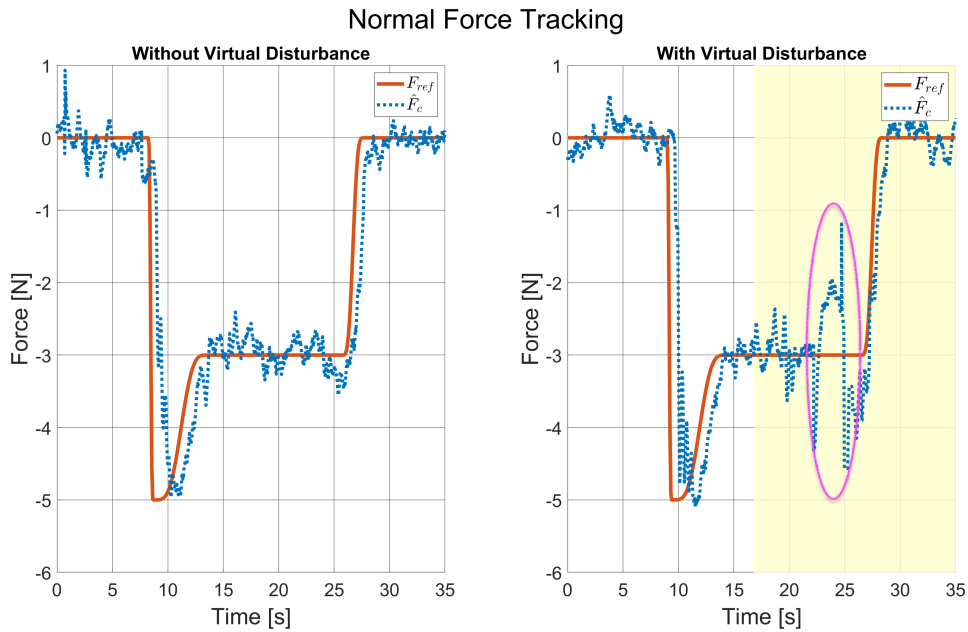
Figure 4.10: L-Shaped Trajectory with Fix End-Effector

The system demonstrates a solid ability to estimate and reject force disturbances caused by a virtual source (yellow background) while maintaining a consistent normal contact force against the table. The performance of the EKF algorithm is presented in Figure 4.11.
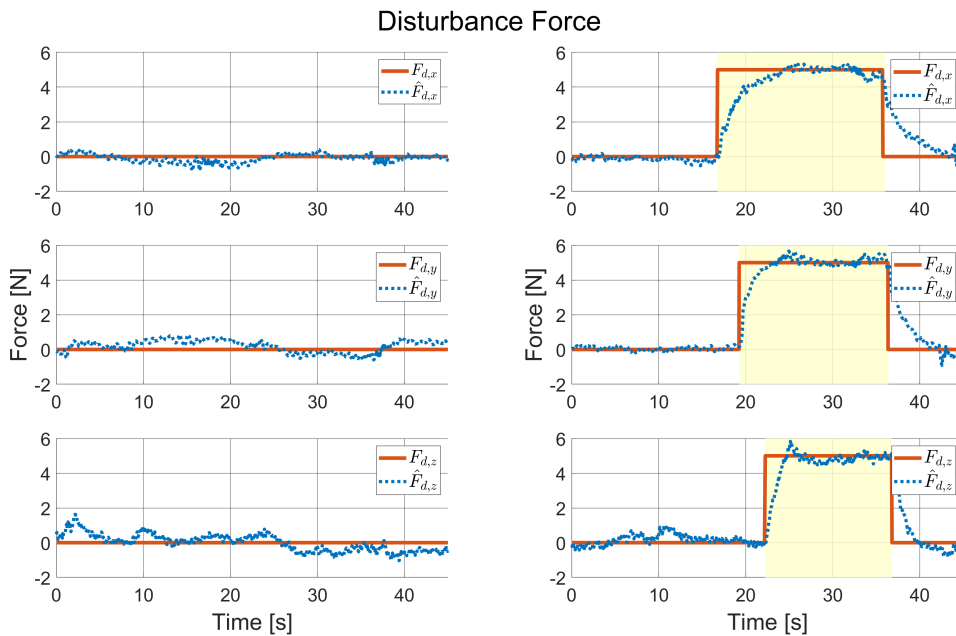

Figure 4.11: L-Shaped Trajectory with Fix End-Effector

The EKF wrench estimate responses quickly and converges accurately to the corresponding virtual disturbances. Therefore, we can qualitatively validate the EKF algorithm for disturbance wrench estimation. Additionally, due to the fast response

of the EKF, the platform can counter react to the occurring disturbances, such we do not observe a meaningful decrease in the force tracking performance.

Moving End-Effector

This experiment evaluates the ability of configuration with a delta arm to perform more advanced interaction tasks. The objective is still to exert the desired normal force to the surface. But now, the flying base should remain at the same position, and only the end-effector moves along its desired trajectory relative to the robot body. Here, the planner traces a triangular trajectory for the end-effector along the table while the vehicle base position and orientation are fixed in the world global frame. The system is autonomously positioned to a start point and aligns with the normal interaction surface axis, then autonomously approaches the workpiece to exert a specific contact force. As contact is made the end-effector starts to slide along the table surface.

In Figure 4.12, we depict the normal force tracking performance. It is visible that the performance is worse than it was for a fixed end-effector scenario (see Fig 4.10), but the robot is able to fulfil its objective task, namely to track the desired normal force.
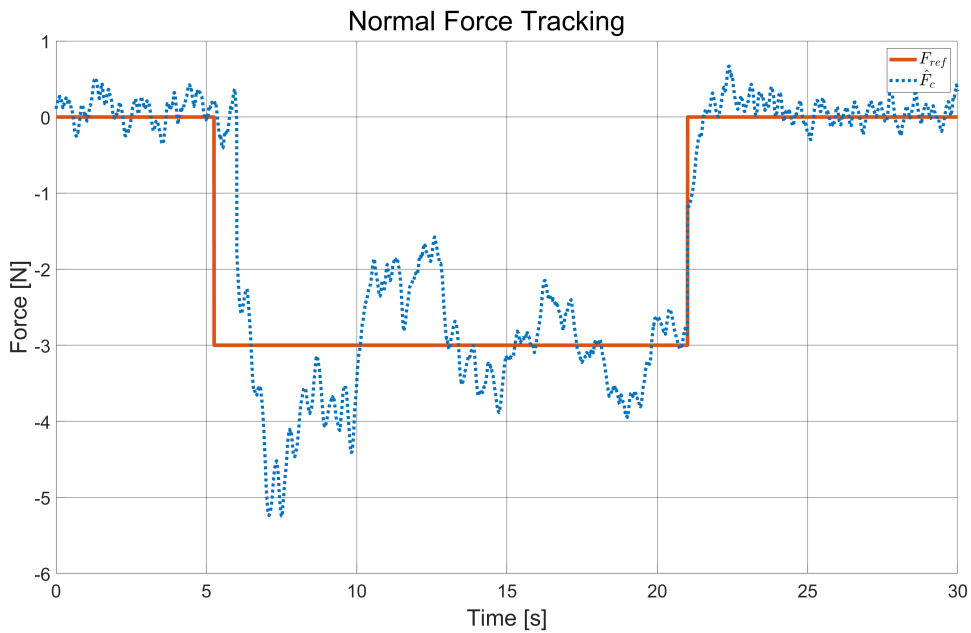

Figure 4.12: End-Effector Moving along a Triangular Trajectory. The EKF normal force estimate is plotted in blue, while the reference is in orange.

4.4.3   Interaction with Rigid Manipulator

The upcoming experiments will focus on showcasing the proposed framework capabilities while the simple rigid manipulator is attached to the platform.

Sliding Along Consecutive Workpieces

To show that the platform can interact with the environment while not being aligned to the contact surface and perform advanced tasks with subsequent workpieces, we

present the following experimental setup, as depicted in Figure 4.13.
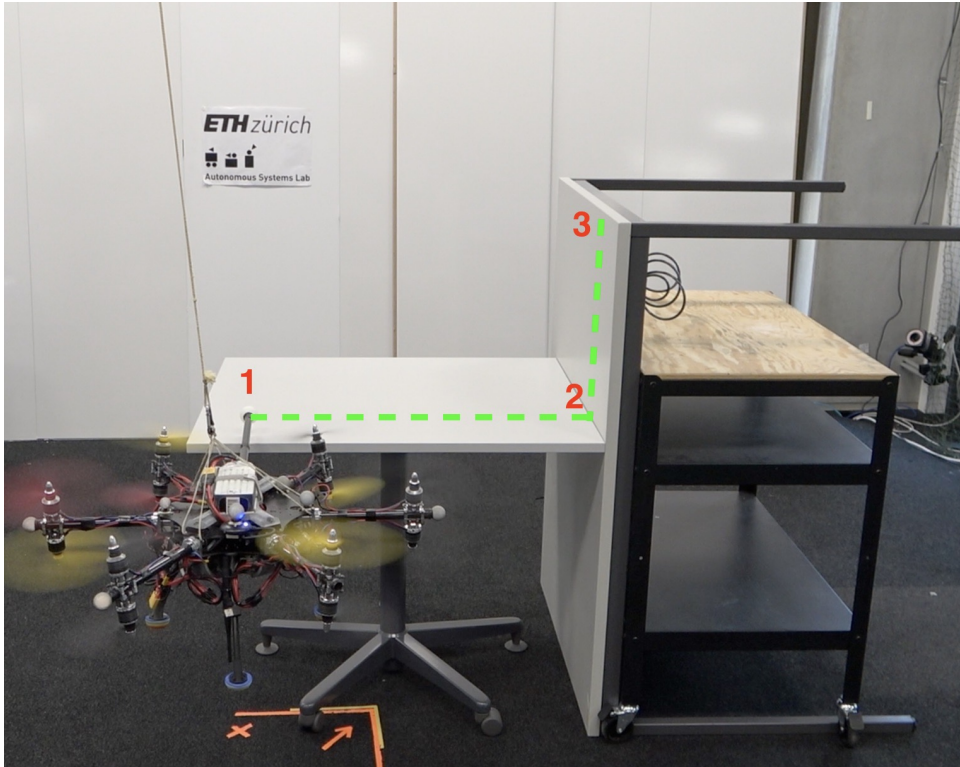

Figure 4.13: Experimental Setup for OMAV with Rigid Manipulator

We put in an extra table vertically to get interaction surfaces which stay perpendicular to each other. Additionally, as presented in the image, the vehicle is not aligned with the normal direction of either workpiece. In the Figure, we depict the desired trajectory of the end-effector while sliding along the consecutive workpiece surfaces. The entire path is performed autonomously by the vehicle and reads:

$$\text{Free Flight} \; \rightarrow 1 \; \rightarrow \; 2 \; \rightarrow \; 3 \; \rightarrow \; 2 \; \rightarrow \; 1 \rightarrow \; \text{Free Flight}$$

Virtual Disturbance

In the first experiment, the system executes the above-defined trajectory twice. The objective is to track the desired normal force reference to the surface while interacting with multiple workpieces along the path. At the time of the second run (yellow background in Figure 4.14), we perturbed the flying platform with the virtual three-dimensional force. Thus, we aim to show the ability of the framework to distinguish between external wrenches acting on the vehicle. Simultaneously, the system rejects continuously the occurring disturbances based on the actual EKF disturbance wrench estimate.

It is visible that the framework can accurately and with short response time estimate the current disturbance forces. Thus, the platform performance is not affected significantly by occurring virtual disturbances as they result in temporary position changes less than 0.05 m, as depicted in Figure 4.15. Applying virtual disturbance during interaction verifies that the platform differentiates between interaction and
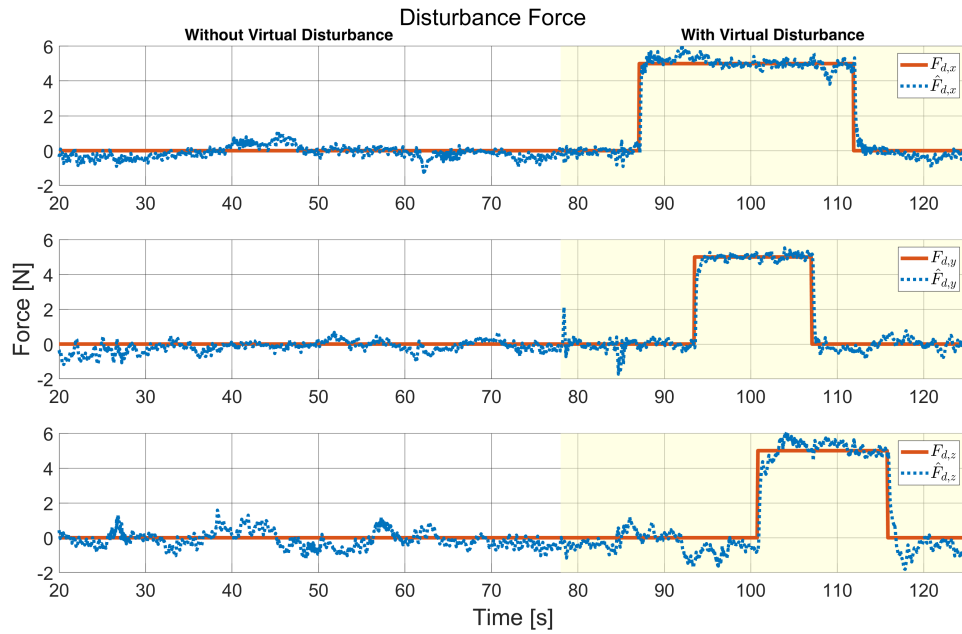
Figure 4.14: Interaction with Multiple Workpieces - Virtual Disturbance

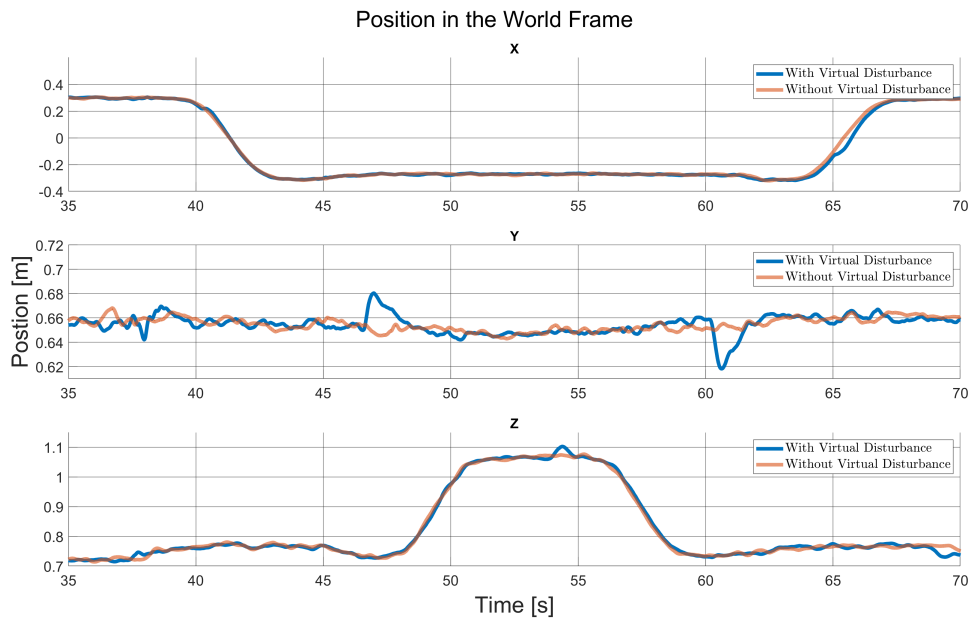disturbance wrenches appropriately and reliably estimates their quantities.

Figure 4.15: Interaction with Multiple Workpieces - Virtual Disturbance

In Figure 4.16, we present the normal force tracking performance for these scenarios. The trajectory execution of both attempts is very similar. Additionally, the tracking has not been strongly influenced by the virtual disturbance. The four peaks in both scenarios correspond to the transition phase between consecutive workpieces (Set-point 2 in Figure 4.13). Although the vehicle is not aligned with its interaction surface, the system tracks the desired normal force reference without any offset. The platform uses only one-directional force such that it does not lose the position

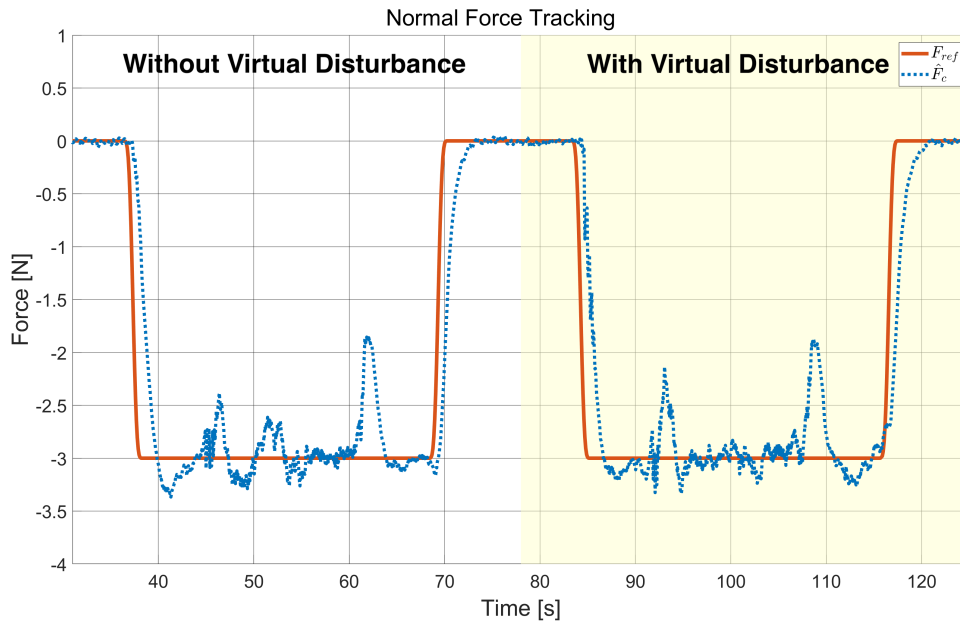authority and can slide along the interaction surface in any direction.

Figure 4.16: Interaction with Multiple Workpieces - Virtual Disturbance

Wind Disturbance

In the last segment of this chapter, we wish to demonstrate a vehicle's performance under physical conditions which can occur in real-world scenario. Instead of virtual disturbance, a wind fan generates an air disturbance, as shown in Figure 4.17. We perform the two tests in a row, first while the wind fan is active and the second while the device is switched off. The objective remains the same as before, i.e. the flying robot should track the normal force reference along the consecutive workpieces, be able to distinguish between external wrenches, and reject only the disturbance.
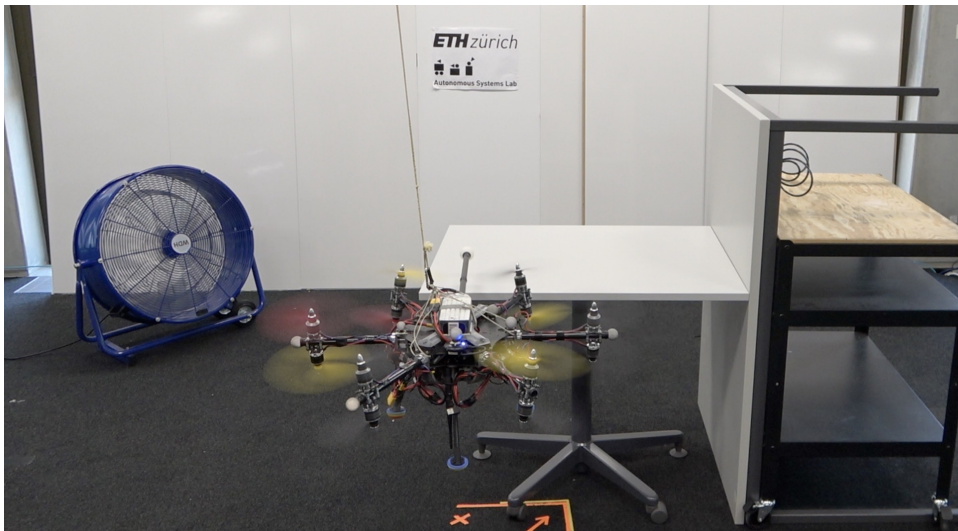

Figure 4.17: Interaction with Multiple Workpieces - Wind Disturbance

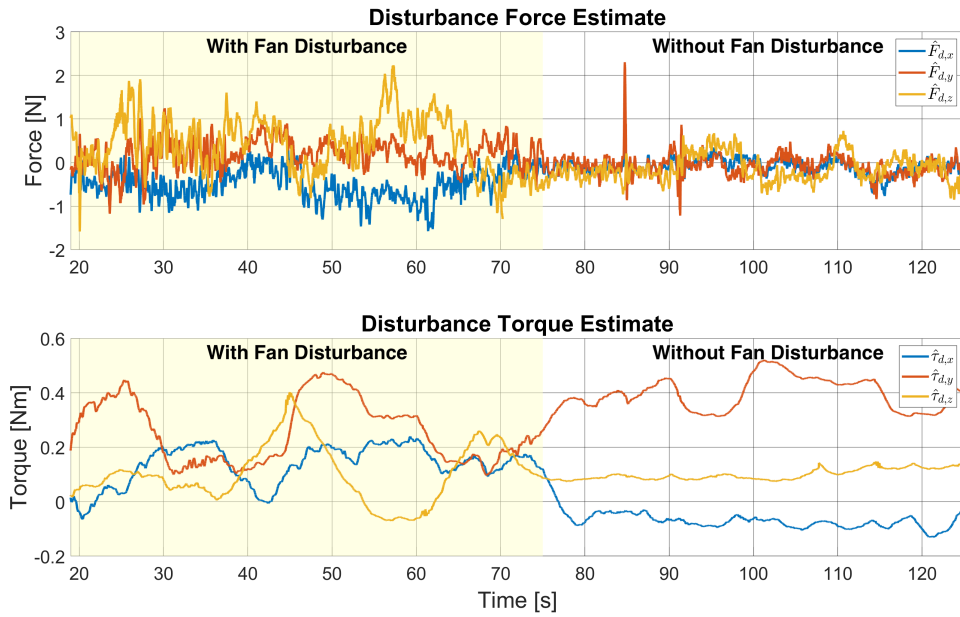First, we present the EKF disturbance wrench estimate in fig 4.18.

Figure 4.18: Interaction with Multiple Workpieces - Wind Disturbance

The yellow background highlights the period when the wind fan was active. It turns out that the air disturbance mainly induced an external disturbance torque on the platform. After switching off the fan, the force and torque disturbance estimates converge to their steady-state values. Offsets in x-, y- and z-torque are the result of the modelling errors in the offset of the vehicle's centre of mass.

For reference, we depict the orientation (fig. 4.19) and position (fig. 4.20) of the vehicle for this experiment.
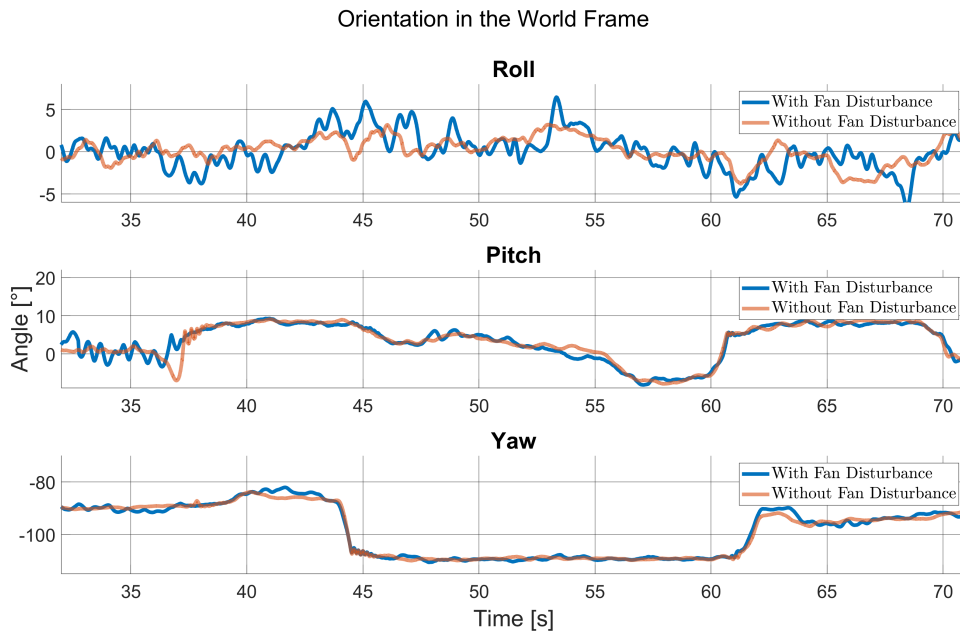

Figure 4.19: Interaction with Multiple Workpieces - Wind Disturbance

The plots marked in blue correspond to the duration while the wind fan was generating an air disturbance, and we show the system pose while no external disturbances are acting on the flying robot in orange.
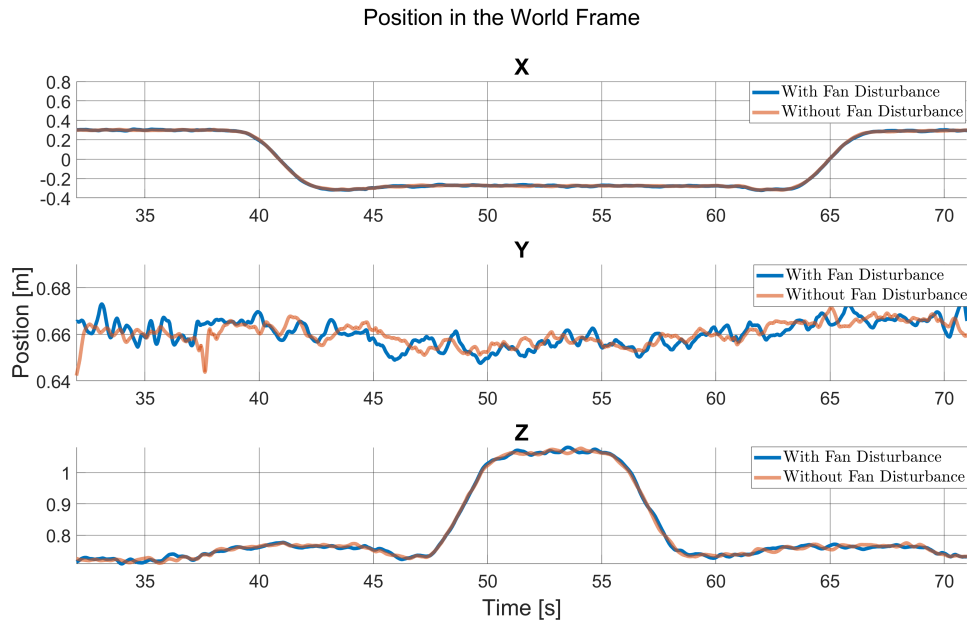

Figure 4.20: Interaction with Multiple Workpieces - Wind Disturbance

This experiment demonstrates that the proposed Hybrid Motion/Force Controller with EKF Wrench Estimator can compensate right for external disturbance, maintaining attitude error within 0.08 rad.

Finally, we present the normal force tracking performance in Figure 4.21.
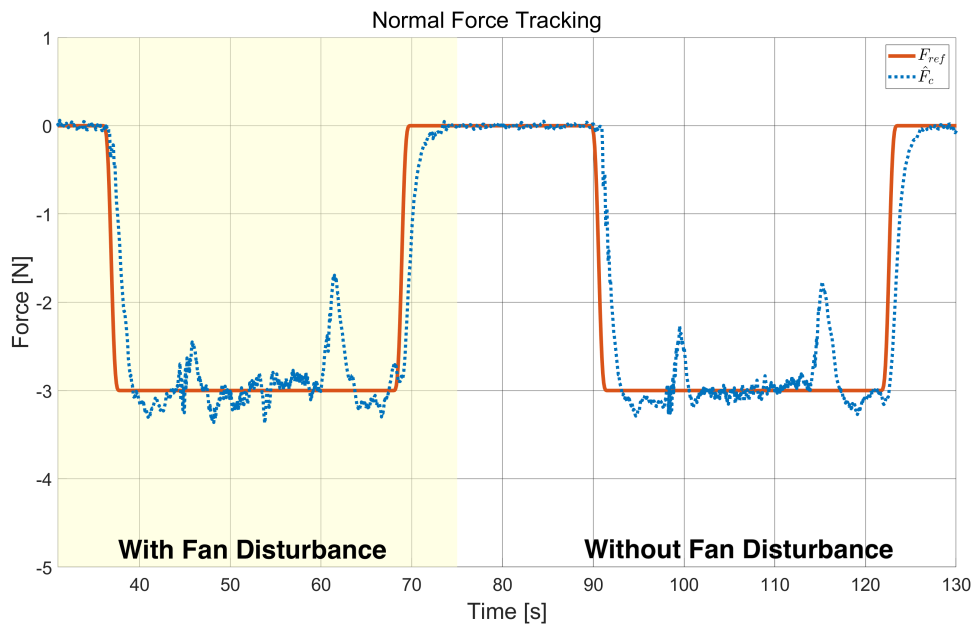

Figure 4.21: Interaction with Multiple Workpieces - Wind Disturbance

It is remarkable that the controller approach is robust and does not experience much difference in the tracking performance, although in the first period the air disturbance acted on the flying system.

The performance of the EKF estimation framework presented in this chapter demonstrates that the platform can reliably distinguish between external wrenches acting on the system. Simultaneously, thanks to the Hybrid Motion/Force Controller, the flying vehicle can fulfil its interaction task while sliding along consecutive workpieces and exert reference force in any direction of the body frame.

Chapter 5

Conclusion

In conclusion, this report presented an algorithm to estimate and distinguish between external forces and torques acting on an over-actuated flying vehicle (OMAV). We showed that the proposed algorithm adequately handles noisy measurements, requires only a few intuitive covariance values to be tuned, and can serve as a basis for reacting to aerodynamic perturbations without relying on specialized knowledge of the underlying dynamics of the disturbance or of the aerodynamic properties of the platform, or on specialized sensors for measuring wind speed. We have demonstrated in the experiments how the external wrench estimate may be used in conjunction with a Hybrid Motion/Force controller to enable an OMAV to hold a position even in the presence of a wind source while also interacting with the environment.

The achievements of the project can be summarized as follows:

- The designed framework enables the system to distinguish between interaction and disturbance wrenches and reliably estimates their current values.

- Based on the obtained EKF wrench estimate, the system is able to reject external disturbances.

- We extended the flying vehicle capabilities to track precisely and offset free the desired interaction force even while external disturbances occur. The platform gained a novel ability to track reference forces in any direction of the body frame. With the Hybrid Motion/Force controller, the flying robot adjusts its position and attitude with respect to the interaction surface to exert desired force accordingly.

- The presented framework can be applied with any manipulator type. Our approach only assumes that there is one interaction point with the environment. We demonstrated the framework capabilities with the delta parallel arm in addition to the simple rigid manipulator.

Chapter 6

Future work

At this point, the possible improvements and future work should be discussed.

- During the experiments, we find out the limits for the interaction force that the platform can track are $[2, 10]$N. One could investigate methods to increase and go beyond those interaction force boundaries. Enabling tracking of even lower interaction forces seems to be a demanding next research topic.

- The transition phase, i.e. the transition between free-flight and interaction and the transition between subsequent interaction workpieces is still to improve. In such a way that there is no significant loss of the force tracking in the normal direction. The possible solution could be to use a compliant element at the tip of the manipulator. Thus, the platform could gain the capability to track even lower forces than the limit defined above. Additionally, introducing the compliant element may decrease the noisy nature of the raw F/T sensor reading and enhance the flying platform to cope with the bumping effect upon contact.

- As all experiments were conducted in a fully controlled laboratory environment, the next step should be to reproduce those experiments in outdoor conditions. Thus the platform would be not able to get precise pose measurements from the camera motion capture system, and the odometry would need to rely on the IMU readings only. Possibly, one could equip the platform with other sensors, like GPS, to enhance odometry state estimates.

- The possible extension of the demonstrated framework is to estimate the actual interaction point between the aerial manipulator and the environment. Thus, one could get rid of an assumption of one single interaction point and perform even more advanced interaction tasks or use a more complex type of manipulator attached to the flying base.

Bibliography

[1] K. Bodie, M. Brunner, M. Pantic, S. Walser, P. Pfändler, U. Angst, R. Siegwart, and J. I. Nieto, "An omnidirectional aerial manipulation platform for contact-based inspection," *CoRR*, vol. abs/1905.03502, 2019.

[2] G. Darivianakis, K. Alexis, M. Burri, and R. Siegwart, "Hybrid predictive control for aerial robotic physical interaction towards inspection operations," in *2014 IEEE International Conference on Robotics and Automation (ICRA)*, 2014, pp. 53–58.

[3] L. Marconi and R. Naldi, "Control of aerial robots: Hybrid force and position feedback for a ducted fan," *IEEE Control Systems Magazine*, vol. 32, no. 4, pp. 43–65, 2012.

[4] A. Albers, S. Trautmann, T. Howard, T. A. Nguyen, M. Frietsch, and C. Sauter, "Semi-autonomous flying robot for physical interaction with environment," in *2010 IEEE Conference on Robotics, Automation and Mechatronics*, 2010, pp. 441–446.

[5] N. Sydney, B. Smyth, and D. A. Paley, "Dynamic control of autonomous quadrotor flight in an estimated wind field," in *52nd IEEE Conference on Decision and Control*, 2013, pp. 3609–3616.

[6] D. Yeo, N. Sydney, D. Paley, and D. Sofge, "Onboard flow sensing for downwash detection and avoidance with a small quadrotor helicopter," 01 2015.

[7] B. Chan, J. Jo, and M. Blumenstein, "Towards uav-based bridge inspection systems: A review and an application perspective," *Structural Monitoring and Maintenance*, vol. 2, pp. 283–300, 09 2015.

[8] P. Pfändler, K. Bodie, U. Angst, and R. Siegwart, "Flying corrosion inspection robot for corrosion monitoring of civil structures – first results," in *SMAR 2019 - Fifth Conference on Smart Monitoring, Assessment and Rehabilitation of Civil Structures - Program.* S.l.: SMAR, 2019-08, p. We.4.A.6, sMAR 2019 – 5th Conference on Smart Monitoring, Assessment and Rehabilitation of Civil Structures; Conference Location: Potsdam, Germany; Conference Date: August 27-29, 2019; Paper presented on Wednesday, 28. August, 2019.

[9] T. Tomić and S. Haddadin, "A unified framework for external wrench estimation, interaction control and collision reflexes for flying robots," in *2014 IEEE/RSJ International Conference on Intelligent Robots and Systems*, 2014, pp. 4197–4204.

[10] F. Ruggiero, J. Cacace, H. Sadeghian, and V. Lippiello, "Impedance control of vtol uavs with a momentum-based external generalized forces estimator," in *2014 IEEE International Conference on Robotics and Automation (ICRA)*, 2014, pp. 2093–2099.

[11] K. Bodie, M. Brunner, M. Pantic, S. Walser, P. Pfändler, U. Angst, R. Siegwart, and J. Nieto, "Active interaction force control for contact-based inspection with a fully actuated aerial vehicle," *IEEE Transactions on Robotics*, vol. 37, no. 3, pp. 709–722, 2021.

[12] H.-N. Nguyen and D. Lee, "Hybrid force/motion control and internal dynamics of quadrotors for tool operation," in *2013 IEEE/RSJ International Conference on Intelligent Robots and Systems*, 2013, pp. 3458–3464.

[13] S. Park, J. Lee, J. Ahn, M. Kim, J. Her, G.-H. Yang, and D. Lee, "Odar: Aerial manipulation platform enabling omnidirectional wrench generation," *IEEE/ASME Transactions on Mechatronics*, vol. 23, no. 4, pp. 1907–1918, 2018.

[14] H. W. Wopereis, J. J. Hoekstra, T. H. Post, G. A. Folkertsma, S. Stramigioli, and M. Fumagalli, "Application of substantial and sustained force to vertical surfaces using a quadrotor," in *2017 IEEE International Conference on Robotics and Automation (ICRA)*, 2017, pp. 2704–2709.

[15] R. Naldi, A. Macchelli, N. Mimmo, and L. Marconi, "Robust control of an aerial manipulator interacting with the environment**this work has been partially supported by the european project airborne (ict 780960)." *IFAC-PapersOnLine*, vol. 51, no. 13, pp. 537–542, 2018, 2nd IFAC Conference on Modelling, Identification and Control of Nonlinear Systems MICNON 2018.

[16] B. Yüksel, C. Secchi, H. H. Bülthoff, and A. Franchi, "Aerial physical interaction via ida-pbc," *The International Journal of Robotics Research*, vol. 38, no. 4, pp. 403–421, 2019.

[17] P. Chermprayong, K. Zhang, F. Xiao, and M. Kovac, "An integrated delta manipulator for aerial repair: A new aerial robotic system," *IEEE Robotics Automation Magazine*, vol. 26, no. 1, pp. 54–66, 2019.

[18] K. Bodie, M. Tognon, and R. Siegwart, "Dynamic end effector tracking with an omnidirectional parallel aerial manipulator," *IEEE Robotics and Automation Letters*, vol. 6, no. 4, pp. 8165–8172, 2021.

[19] J. Solà, "Quaternion kinematics for the error-state kf," 03 2015.

[20] C. Richter, A. Bry, and N. Roy, "Polynomial trajectory planning for aggressive quadrotor flight in dense indoor environments," in *Robotics Research.* Springer, 2016, pp. 649–666.

[21] M. Burri, H. Oleynikova, , M. W. Achtelik, and R. Siegwart, "Real-time visual-inertial mapping, re-localization and planning onboard mavs in unknown environments," in *Intelligent Robots and Systems (IROS 2015), 2015 IEEE/RSJ International Conference on*, Sept 2015.

[22] O. Khatib, "A unified approach for motion and force control of robot manipulators: The operational space formulation," *IEEE Journal on Robotics and Automation*, vol. 3, no. 1, pp. 43–53, 1987.

[23] K. Bodie, Z. Taylor, M. Kamel, and R. Siegwart, "Towards efficient full pose omnidirectionality with overactuated mavs," *CoRR*, vol. abs/1810.06258, 2018.